

©2018

He Zhang

ALL RIGHTS RESERVED

ANALYSIS OF PRESTRESSED CONCRETE BRIDGES WITHOUT PLANS

by

HE ZHANG

A thesis submitted to the

School of Graduate Studies

Rutgers, The State University of New Jersey

in partial fulfillment of the requirements

for the degree of

Master of Science

Graduate Program in Civil and Environmental Engineering

written under the direction of

Dr. Hani H. Nassif

and approved by

New Brunswick, New Jersey

May 2018

ABSTRACT OF THE THESIS

ANALYSIS OF PRESTRESSED CONCRETE BRIDGES WITHOUT PLANS

By HE ZHANG

Thesis Director:

Dr. Hani H. Nassif

Evaluation of prestressed concrete bridges requires the calculation of the load rating factor, which is an indicator for the assessment of the current load carrying capacity. To calculate the rating factors (RFs), there is a need to know the geometries and current deterioration of various bridge elements. Moreover, for bridges that are old and without plans, a methodology is needed to estimate the rating factors and give guidance for future assessment and inspection of these bridges.

The objective of this thesis is to develop guidelines on how to load rate prestressed concrete (P/C) girder bridges without plans. The guidelines include data collection, use of nondestructive testing/evaluation (NDT/E) and load tests, as well as a proposed approach to estimate the as-built design. To validate the proposed approach, nine (9) simply-supported P/C girder bridges with known plans were selected for this study. Diagnostic load test and NDT/E were performed on a simply supported P/C I-girder bridge located on I-80 Eastbound over Mount Hope Mineral Railroad. A 3-axles Class 6 truck, with a gross vehicle weight (GVW) of 54.7 kips, was utilized for the field testing of the bridge. The field tests were performed when the truck was traveling at highway speed as well as

crawling speed. Strains caused by the truck traveling across the bridge were collected and used to calculate the girder distribution factors (GDFs). The GDFs based on the load test, were compared to those calculated from the American Association of State Highway and Transportation Officials (AASHTO) Specification GDF equations and found to be conservative. Additionally, the Schmidt Hammer and the Ground Penetrating Radar (GPR) were also used to estimate the compressive strength of concrete and shear reinforcement spacing, respectively. The minimum requirement of the prestressed tendons was determined by the Magnel Diagram (i.e., feasibility domain) analysis using the original design loads. The results showed that the number of tendons for all nine (9) bridges specified in the plans fall in the range that was estimated by the Magnel Diagram. With this proposed approach, lower bound and upper bound values of the load rating factors for each bridge were estimated. The approach was also applied to calculate the flexural and shear capacities when deterioration was identified.

ACKNOWLEDGMENTS

I would like to thank my advisor, Dr. Hani Nassif, for his continuous support throughout my study at Rutgers. It has been a great honor for me to have him as my advisor, who is always there giving me guidance, encouragement, and knowledge.

I would like to thank Dr. Husam Najm and Dr. Hao Wang for being on my thesis committee and their valuable advice.

I would like to thank the research associate, Dr. Peng Lou, for helping me start my study in RIME group, also for being as a mentor, who would teach me things in all aspects.

I would like to thank my work colleagues, graduate assistant, Thanachai Srithaninrat, Dongjian Gao, Jonathan Rodriguez, research associate Dr. Chaekuk Na, post-doctoral associate Dr. Changhee Park, and Dr. Graziano Fiorillo, and visiting student, Enson Portela and for their helpful suggestion, fruitful discussion and also being my friends. Their experiences in life and engineering filed help me get through all the obstacles during my work. They create a harmonious atmosphere with fun for the people working here.

I would like to thank Engineers from NJDOT, Mula Reddy, Eddy Germain, Fan Zhuo and Nishit Patel, for their insights and supports on BRP project.

I would like to thank my father and mother who always give me unconditionally love, cares and supports. They help me grow and shape me into the person I am today.

TABLE OF CONTENTS

ABSTRACT OF THE THESIS	ii
ACKNOWLEDGMENTS	iv
TABLE OF CONTENTS.....	v
LIST OF FIGURES	viii
LIST OF TABLES.....	xi
1. Introduction.....	1
1.1. Background.....	1
1.2. Objectives	2
2. Literature Review.....	4
2.1. General Load Rating Procedures of AASHTO Manual for Bridge Evaluation (MBE)	4
2.2. General Studies on Load Rating for Prestressed Concrete without Plans	6
2.3. General Studies on Load Test.....	11
2.4. Load Rating of Prestressed Concrete Bridges with Deterioration.....	13
3. Field Testing	15
3.1. Field Visit of Bridge with Structure Number 1412178	15
3.2. Diagnostic Load Test	16
3.2.1. Structural Testing System.....	17
3.2.2. STS Instrumentation and Testing Plan	20

3.2.3. Calibration Truck	22
3.2.4. Diagnostic Load Test	23
3.2.5. Validation of Non-Destructive Test Tools.....	26
3.3. Test Results	29
4. Analysis of bridges without Plans.....	38
4.1. Analysis of Bridges Known Plans	38
4.1.1. Information Collection.....	38
4.1.2. Validation of Load Rating Procedure	39
4.1.3 Load Rating Bridges with Structure Number #1412-178	43
4.2. Results from Testing Data.....	44
4.2.1. NDT/E Results	45
4.2.2. Neutral Axis Analysis	46
4.2.3. Strain Results Comparison and Girder Distribution Factor (GDF)	49
4.2.4. Load Effect and Posting Load.....	53
4.3. Analysis of Bridges without Plans	54
4.4. Comparison of Load rating Results.....	63
4.5. Capacity Comparison in Bridge Inventory	65
4.5.1. Bridge Inventory and Re-design	65
4.5.2. Bridge Inventory and Profile	74
4.5.3. Capacity Comparison.....	78

4.6. Analysis of Deteriorated Bridges with No Plans	80
4.6.1. Field Visit of Bridges with Structural Number 1412-178	80
4.6.2. Analysis of Bridges with Deterioration for #1412-178	82
4.6.3. Information in Cycle Report of #1420-168 (End-Span)	83
4.6.4. Analysis of the Bridge with Deterioration for #1420-168 (End-Span).....	83
4.6.5. Analysis of Bridges with Deterioration for #1413-156	85
5. Conclusions and Summary	87
5.1. Conclusion	87
5.2. Future Work	90
References	91

LIST OF FIGURES

Figure 1. Load and Resistance Factor Rating Flow Chart (AASHTO MBE 2 nd Edition) ..	6
Figure 2. Field Condition of #1412178.....	16
Figure 3 Bridge #1412178 Location	17
Figure 4. Wireless Data Collection System, Bridge Diagnostics Inc.	18
Figure 5. Sensors Installation.....	19
Figure 6. STS Strain Transducer Installed on a Bridge Superstructure Member	19
Figure 7. Typical Sensor Locations	20
Figure 8. Layout of Sensors	21
Figure 9. Strain Transducers Location and Number	22
Figure 10. Weighing Procedure for Calibration Truck.....	22
Figure 11. Calibration Truck.....	23
Figure 12. Sensor Installation	24
Figure 13. Diagnostic Load Test.....	25
Figure 14. Diagnostic Load Paths.....	25
Figure 15. Raw Strain Data from BDI Software.....	25
Figure 16. Proposed NDT/E tools for field testing; (a) Original Schmidt Hammer and (b) Profoscope+ (rebar locator)	26
Figure 17. Sample A (a) Statistical Results (b) Comparison of Schmidt Hammer and Compression Machine.	28
Figure 18. Measured Strain Data for PATH 1 / Girder G4.....	30
Figure 19. Measured Strain Data for PATH 1 / Girder G5.....	31
Figure 20. Measured Strain Data for PATH 1 / Girder G6.....	31

Figure 21. Measured Strain Data for PATH 2 / Girder G3.....	32
Figure 22. Measured Strain Data for PATH 2 / Girder G4.....	32
Figure 23. Measured Strain Data for PATH 2 / Girder G5.....	33
Figure 24. Measured Strain Data for PATH 3 / Girder G2.....	33
Figure 25. Measured Strain Data for PATH 3 / Girder G3.....	34
Figure 26. Measured Strain Data for PATH 3 / Girder G4.....	34
Figure 27. Measured Strain Data for PATH 4 / Girder G1.....	35
Figure 28. Measured Strain Data for PATH 4 / Girder G2.....	36
Figure 29. Measured Strain Data for PATH 4 / Girder G3.....	36
Figure 30. Measured Strain Data for PATH 4 / Girder G4.....	37
Figure 31. Cross-section of the Girder.....	38
Figure 32. Our Rating Spreadsheet Parameter.....	40
Figure 33. MBE Rating Spreadsheet Parameter	41
Figure 34 GPR Results (Photo provided by AID Inc.)	45
Figure 35. Schmidt Hammer Testing (Photo provided by AID Inc.)	46
Figure 36. Guideline for Load Rating Assessment of Bridges without Plans	54
Figure 37. Feasibility Domain	56
Figure 38. Feasibility Domain for HS-20	57
Figure 39. New Design Section	58
Figure 40. Feasibility Domain for HL-93	62
Figure 41. Feasibility Domain for #0235-157	66
Figure 42. Feasibility Domain for #0235-156	67
Figure 43. Summary of Rating Factor Using HL-93 (Bridge #0235-156)	67

Figure 44. Feasibility Domain for #1420-168 Middle span	68
Figure 45. Feasibility Domain for #1420-168 End span.....	69
Figure 46. Feasibility Domain for #1413-156	70
Figure 47. Feasibility Domain for #0327-150	71
Figure 48. Feasibility Domain for #1016-159	72
Figure 49. Feasibility Domain for #2113-153	73
Figure 50. AASHTO Type V # 0235-157	74
Figure 51. AASHTO Type V # 0325-156	74
Figure 52 AASHTO Type II # 1412-178.....	75
Figure 53. AASHTO Type III # 1420-168 Middle Span.....	75
Figure 54. AASHTO Type I # 1420-168 End-Span	75
Figure 55. AASHTO Type II # 1413-156.....	76
Figure 56. AASHTO Type II # 0327-150.....	76
Figure 57. AASHTO Type II # 1016-159.....	76
Figure 58. AASHTO Type II # 2113-153.....	77
Figure 59. Deterioration at Support	81
Figure 60. Exposed Tendons in 1412-178	81
Figure 61. Exposed Tendons in 1420-168 (End-Span).....	83
Figure 62. Exposed Tendons in 1413-156	85

LIST OF TABLES

Table 1. - Condition Factor in MBE	13
Table 2. - Condition States.....	14
Table 3. - Inventory of the Sensor Instrumentation underneath the Superstructure	21
Table 4. - Strength estimation of Schmidt Hammer	29
Table 5. Rating Example 1 MBE.....	40
Table 6. Rating Example 2 WisDOT Bridge Manual.....	41
Table 7. Design Example 1 PCI.....	42
Table 8. Design Example 2 FHWA	42
Table 9 Summary of Moments and Shears (Given Plans).....	43
Table 10. Rating Factor for Bridge Structure #1412-178 Based on Given Plans.....	44
Table 11. Neutral Axis (from bottom flange) Data with the Corresponding Path.....	46
Table 12. - Distribution Factors Based on Load Test	50
Table 13. - Summary of Maximum GDFs	51
Table 14. - Calculated GDFs Using AASHTO Specification [11].....	52
Table 15. - Load effect comparison between Legal load and calibration truck.....	53
Table 16. Four Stress Inequality Equations	55
Table 17. - Rating Factor for Re-design (re-design with 18 tendons)	58
Table 18. - Summary of Moments and Shears (re-design)	59
Table 19. Rating Factor for Re-design (re-design with 36 tendons).....	60
Table 20. - Sensitivity Study Summary	61
Table 21. - Summary of Rating Factor Using HL-93 (Bridge #1412-178)	64
Table 22. Summary of Rating Factor Using HL-93 (Bridge #0235-157).....	66

Table 23. Summary of Rating Factor Using HL-93 (Bridge #1420-168, middle span) ...	68
Table 24. Summary of Rating Factor Using HL-93 (Bridge #1420-168, end span)	69
Table 25. Summary of Rating Factor Using HL-93 (Bridge #1413-156).....	70
Table 26. Summary of Rating Factor Using HL-93 (Bridge #0327-150).....	71
Table 27. Summary of Rating Factor Using HL-93 (Bridge #1016-159).....	72
Table 28. Summary of Rating Factor Using HL-93 (Bridge #2113-153).....	73
Table 29. Summary of Structure and Capacity	79
Table 30. RFs of Minimum Design for 1412-178 without Deterioration (18 tendons)....	82
Table 31. RFs of Minimum Design for 1412-178 with Deterioration (16 tendons).....	82
Table 32. RFs of Minimum Design for 1412-178 without Deterioration (4 tendons).....	84
Table 33. RFs of Minimum Design for 1412-178 with Deterioration (3 tendons).....	84
Table 34. RFs of Minimum Design for 1413-156 without Deterioration (29 tendons)....	85
Table 35. RFs of Minimum Design for 1413-156 with Deterioration (28 tendons).....	86

Chapter I

1. Introduction

1.1. Background

With the development of prestressed concrete (P/C) in the early twentieth century, many bridges were built in the 1960s and 1970s using prestressed girders. However, as the time passes, bridges have seen heavier loads than the original design load, and those bridges eventually started to deteriorate and became structurally unstable. The conditions of those bridges became worse, and their load carrying capacity raised major concerns for local agencies. Rating factor (RF) was introduced to evaluate the existing bridges during the cyclical inspection. For the bridges with plans, the rating factors (RFs) can be calculated to indicate the safety level. However, there are some bridges that are old and lack of as-built drawing information. Because the prestressing tendons and reinforcement are embedded in concrete, without plans, the load carrying capacity are difficult to be determined. The resistance can be only estimated by engineering judgment, or sometimes, it might not be stated in the inspection report. In this study, a new methodology of load rating procedure is proposed to estimate the rating factors of P/C girder bridges when plans are not available.

To calculate the rating factors conservatively, several approaches were used. For a target bridge with no plans, if no major deterioration is found, the first step is to re-design the bridge with Magel Diagram (i.e., feasibility domain). The re-design must be done

according to the live load model during the period when the bridge was built. Using this approach, the required number of tendons can be determined, and to be conservative, the minimum number of tendons is selected. Then, using the minimum design along with the nondestructive testing/evaluation (NDT/E) from the field, the refined RFs can be calculated for a target structure. It should be noted that all rating factors in this study for bridges with no deterioration are calculated with the assumption that the bridges have both condition factor and system factor of one (1.0). If the RFs do not meet the criteria ($RFs < 1$), the diagnostic load test will be performed for analysis, regarding girder distribution factors (GDFs), sensitivity analysis of strands, analysis of neutral axis, and estimation of carrying capacity. Thus, one bridge can be better load rated with the actual structural behavior, and data collected from the field. Load posting for proof load and finite element model would be needed when the RFs are still not satisfied the criteria. The results will give a guideline for preservation, rehabilitation, and load posting if deemed necessary. If the bridge is deteriorated, conservative assumptions should be made based on the conditions of exposed prestressing tendon and concrete. Section losses should be presented in calculations along with the re-design, load test, and NDT/E where the target bridge has a poor or even worse condition.

1.2. Objectives

The main objective of this project is to improve the load rating evaluation for prestressed concrete bridges when plans are not available. From literature, the author reviewed and piloted NDT/E methods and techniques in accordance with the New Jersey Department of Transportation (NJDOT) requirements. The tools were selected, and the feasibility of the

current methodologies and the devices were verified with experiments. The methods and technology would be transferred to NJDOT's Division of Bridge Engineering & Infrastructure Management staff. The rating factors will give guidance to bridge inspection and maintenance.

Chapter II

2. Literature Review

2.1. General Load Rating Procedures of AASHTO Manual for Bridge Evaluation (MBE) [1]

For existing bridges with detailed plans, load rating factors can be examined and calculated followed by AASHTO MBE. The load-rating shall be performed based on a recent and thorough field investigation. If damages or deterioration happened, it might be necessary to lower the capacity. Any rehabilitation or retrofit should be taken into account for calculating and analyzing the condition and load capacity.

Three levels of load-rating were performed in Load and Resistance Factor Rating (LRFR) methodology: 1) design-load rating, 2) legal-load rating, and 3) permit-load rating. Each level indicate different specific targets. Load and Resistance Factor Rating Flow Chart is shown in Figure 1. The general load-rating factor is calculated bt Equation (1):

$$RF = \frac{C - \gamma_{DC}(DC) - \gamma_{DW}(DW) \pm \gamma_P(P)}{\gamma_{LL}(LL + IM)} \quad (1)$$

where

C = capacity

DC = dead load effect due to structural components and attachments

DW = dead load effect due to wearing surface and utilities

P = permanent loads other than dead loads

LL = live load effect

γ_{DC} = LRFD load factor for structural components and attachments

γ_{DW} = LRFD load factor for wearing surfaces and utilities

γ_P = LRFD load factor for permanent loads other than dead loads = 1.0

γ_{LL} = evaluation live load factor

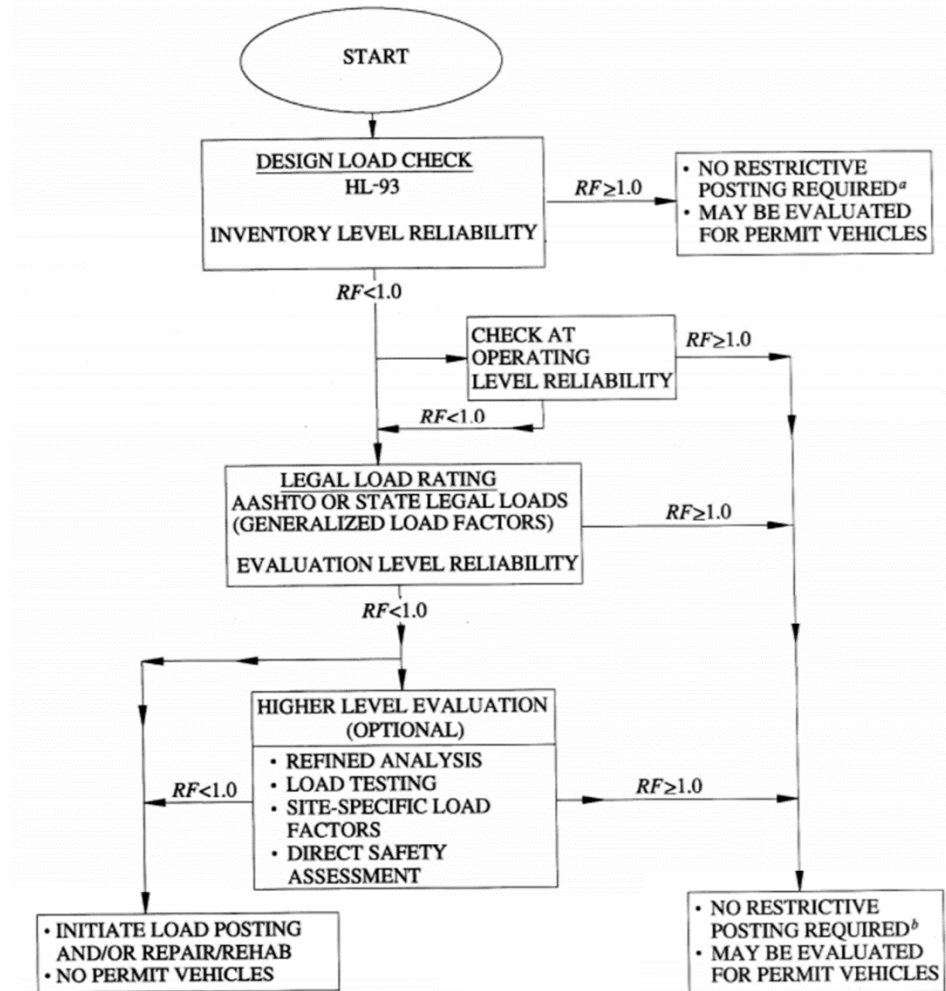


Figure 1. Load and Resistance Factor Rating Flow Chart (AASHTO MBE 2nd Edition)

2.2. General Studies on Load Rating for Prestressed Concrete without Plans

- 2015-Load Rating a Prestressed Concrete Double T-Beam Bridge without Plans by Field Testing- Carlos V. Aguilar et al. [2]

A case study was introduced to present a method of evaluating the load rating of prestressed concrete bridges without plans. From previous work and the procedures in AASHTO

Specification, the proof testing procedures were developed primarily for reinforced concrete at the strength limit state. But considering the essential of analyzing at cracking moment, this study was comparably done at Service III states (concrete cracking) for prestressed concrete.

The four-step load rating procedure:

1. Using the Magnel Diagram to estimate the total number and eccentricity of the prestressing strands based on serviceability criteria for compression and tension at transfer and service.
2. Adopting a rebar scanner, to detect the primary steel reinforcement and verify the estimation from the Magnel Diagram. If the scanner can provide clear images of the rebar, then the bridge can be modeled and analyzed without testing.
3. Gauges were set to measure the strain. A diagnostic load test is performed to measure the beam strains under a truckload approximately 60% of the target proof load. The load test is used to find out the critical transverse truck paths, which generates the largest strains.
4. Fourth, a proof test is conducted to generate the largest possible moment without exceeding the cracking moment.

The adjusted target live load factors (X_{pA}) were calculated for legal load based on the test.

Equations (2) and (3) are shown below.

$$X_{pA} = X_p \left(1 + \frac{\Sigma\%}{100} \right) \quad (2)$$

$$L_T = X_{pA} L_R (1 + IM) \quad (3)$$

where

X_p = initial target load factor,

$\Sigma\%$ = sum of the X_p adjustment factors

L_R = unfactored live load due to the rating vehicle,

IM = impact factor (equal to 1.33).

Operating level capacity can be calculated using Equation (4) as follows:

$$OP = \frac{k_0 L_p}{X_{pA}} \quad (4)$$

where

k_0 = a factor that depends on how the proof test was terminated (1.0 if the target proof moment is reached and 0.88 if the test is stopped because of signs of distress)

L_p = the applied moment.

The rating factor RF_0 can be determined using Equation (5):

$$RF_0 = \frac{OP}{L_R(1 + IM)} \quad (5)$$

- 2015-On-Site Acoustic-Emission Monitoring for Assessment of a Prestressed Concrete Double-Tee-Beam Bridge without Plans- Rafal Anay et al. [3]

Acoustic emission (AE) was used as a supplement in this study to assess the condition of the prestressed concrete bridges during a proof test. It is a nondestructive evaluation (NDE) method that can help monitor the inner condition of the concrete. AE is transient elastic waves generated by energy release in the material from localized sources. AE sensors and strain transducers were set to determine the maximum loading.

During the load test, recording of an AE waveform, a graphical interface of AEwin software was set to show the AE activity versus time for data detected from each channel. It gave a simple indication of damage amount developing near each sensor. The filter was needed to keep the data corresponding to the structural physical response and eliminate undesirable data caused by unrelated factors such as noise wave reflection especially, during the on-site test.

The cumulative signal strength (CSS) parameter and source location techniques have been used to detect cracks and their locations, respectively. The cracking will be found at the location where the AE signals have a high signal strength and sharp changes in the CSS curve slope. The $H(t)$ based on Eq.(6) is a ratio of the cumulative signal strength of recent hits to the cumulative signal strength of all hits. This parameter can be used to estimate the changes in the slope of the cumulative signal strength, which is related to the damages. The severity, S_r in Eq. (7) is calculated based on 50 events.

$$H(t) = \frac{N}{N-K} \frac{\sum_{i=K+1}^N S_{oi}}{\sum_{i=1}^N S_{oi}} \quad (6)$$

$$S_r = \frac{1}{50} \sum_{i=1}^{i=50} S_{oi} \quad (7)$$

where

N = number of hits up to a specific time (t)

S_{oi} = signal strength of the i^{th} event

K = empirically derived factor that varies with the number of hits

One value of K that has been suggested is as follows:

(1) not applicable if $N \leq 50$; (2) $N - 30$ if $51 \leq N \leq 200$; (3) $0.85N$ if $201 \leq N \leq 500$; and (4) $N - 75$ if $N \geq 501$.

The results show that AE is capable of detecting and locating cracks and provide information regarding critical loading paths and conditions and its effect on the performance of the structure.

- 2016-Implementation Plan for Load Rating Prestressed Concrete Bridges without Plans-C.V.Aguilar [4]

The implementation plan combined both analytical (Magnet Diagram) and experimental (Rebar scans, Windsor probe test, field testing) techniques to load rate the bridges. Combining the two method, the rating factors can be more accurately defined. If the rebar scanner cannot confirm the amount and location of the strands, the load testing might be needed. The bridge condition determines the need for load testing. If any damage happened, the load distribution type will be changed, the load test should be performed with cautious. Three case studies were presented on utilizing the implementation plan for the different

type of super-structure types (double T, box, and I-shape). The implementation plan provides factors at both the strength limit state and service limit state based on experimental and analytical load rating methods, respectively. The results from both methods can be compared to select the true load rating factors for each bridge. Engineering judgment is required if the analytical (strength-based) load ratings are lower than the experimental (service-based) load ratings.

2.3. General Studies on Load Test

Joan (2009) did a study for categorizing the load test. Three types of load tests are feasible in bridges: soft, diagnostic, and proof load. [5]

The soft load test uses the actual traffic on the bridge as the loading source. Using a Weigh-In-Motion (WIM) system to obtain the traffic in history. The information about the structural behavior of the bridge can be calculated by statistical data. However, the structure is measured when it is opened to normal traffic. Variances and uncertainties are the major concern for this test. Structure behavior can be calculated for some parameters. If the measurements are sufficiently long, the load history might reflect the structure behavior along the time. This test is aimed to supplement and check the assumptions and simplifications made in the theoretical assessment.

Diagnostic tests are used when validating and adjusting the behavior of an analytical model. In this case, the load is introduced to the bridge with an accurately measured weight. There are two types of diagnostic load tests, static and dynamic. In order to get accurate results,

normally, the target bridge is closed to traffic during the test. When performing both of the two types tests, and comparing the results, information can be obtained for:

1. Impact factor
2. Dynamic parameters (natural frequencies, mode shapes, damping)
3. Load Distribution,
4. Experimental influence lines
5. Girder neutral axis

A proof load test is used when only the structure is insufficient for certain criteria and when a theoretical model cannot reflect the actual structural behavior. Usually, the proof test is heavier than normal load, so that the internal mechanism and response under such load can be observed. It is necessary when the bridge is old and with deterioration, because some elements might not function well and it might lead to some strength or service problem. The proof test can yield to the actual live load capacity of the structure rather than theoretic calculation. However, in such tests, the load introduced in the bridge is relatively high with the risks of damaging the structure, this type of tests is restricted to bridges that have failed to pass the most advanced theoretical assessment. Also, strict observation carried by experienced engineers are needed when posting load to target bridge. The load is increased slowly with certain increment. Any non-linear behavior happen, or response exceeds the limit, the test should be stopped. The objective of this test is to directly obtain the maximum allowable load in the bridge with a required safety level.

2.4. Load Rating of Prestressed Concrete Bridges with Deterioration

- 2011-General load-rating Procedures- AASHTO Manual for Bridge Evaluation (MBE) [1]

According to MBE, the condition factor is used in the equations of rating factor to reflect the overall condition of the structure during inspection.

Table 1 summarizes the condition rating with the corresponding condition factor ϕ_c .

Table 1. - Condition Factor in MBE

Superstructure Condition Rating (SI & A Item 59)	Equivalent Member Structural Condition	ϕ_c
6 or higher	Good or Satisfactory	1.00
5	Fair	0.95
4 or lower	Poor	0.85

- 2015- New Jersey Department of Transportation Bridge Element Inspection Manual [6]

The NJDOT Bridge Element Inspection Manual provides the inspector a guideline to evaluate the condition of the structure. Depending on the degree of deterioration, the structure is graded in terms of Condition States (CS) with the scale of 1-4, are shown in Table 2.

Table 2. - Condition States Rating

Defects	Condition States			
	1	2	3	4
	Good	Fair	Poor	Severe
Exposed Rebar	None.	Present without measurable section loss.	Present with measurable section loss, but does not warrant structural review.	The condition warrants a structural review to determine the effect on strength or serviceability of the element or bridge.
Exposed Prestressing Strand	None.	Present without section loss.	Present with section loss, but does not warrant structural review.	Or a structural review has been completed

Chapter III

3. Field Testing

3.1. Field Visit of Bridge with Structure Number 1412178

A field visit is made to assess the feasibility of performing the load test. Figure 2 shows the overall bridge condition and the surroundings. The bridge is overall in poor condition. Due to accessibility, NDT/E was not able to perform on this structure. Corroded reinforcement and bearing plates were identified at multiple locations. This bridge is crossing over a local route without open traffic. Thus, it is ideal for installing sensors and operating the test without lane closure. Furthermore, the bridge is identified of corrosion, which also can be studied for assessing bridges with deterioration.





Figure 2. Field Condition of #1412178

3.2. Diagnostic Load Test

The goal of load test was to implement proposed load rating procedure on a bridge with a detailed plan. Thus, the results from field testing can be compared with known information. Nondestructive load testing includes diagnostic tests and proof tests. Diagnostic tests can be used to evaluate the actual responses of the structure safely.

Figure 3 shows the location and target bridge. Bridge #1412178, I-80 Eastbound over Mount Hope Mineral Railroad was selected to perform a load test. Only the diagnostic test was performed at this stage to understand the actual behavior and calibrate analytical procedures. Structural responses such strains, and velocity were collected from the load test and will be further used to calculate the distribution of the load, section properties and applied moment.



Figure 3 Bridge #1412178 Location

3.2.1. Structural Testing System

The Structural Testing System (STS) is a modular data acquisition system manufactured by Bridge Diagnostics, Inc. (BDI) of Boulder, Colorado. The system consists of main processing unit, junction boxes, and strain transducers. For concrete structure, the strain transducers are mounted to structural elements with glue and bolted to epoxied tabs for the purpose of non-destructive. Using this system, the sensors can be removed easily after the testing. Each sensor has a unique identification number and a microchip so that it can be identified by the main unit. Each sensor is calibrated and the calibration file is stored in the Toughbook laptop. Main components and the technical specifications of the Wi-Fi system are shown in Figure 4.



Figure 4. Wireless Data Collection System, Bridge Diagnostics Inc.

Each test corresponding to an automatic file number, and the test start to record the strain data by initiating the trigger button called the clicker. Once the test is completed, the data can be downloaded from the STS unit to a Toughbook. The STS data files contain basic test information testing date, time period, transducer ID numbers, and the stress data. Similarly, accelerometers were used to measure the natural frequency of the structure, which is related to the mass and stiffness. The sensors will be connected to STS junction boxes. Loctite 410 and Loctite 7452 aerosol accelerator are used in order to properly mount the sensors to the prestressed girders, per BDI recommendation. Figure 5 shows a strain gauge installed on the bottom flange of the prestressed beam. Figure 6 shows a closer look for a strain gauge.



Figure 5. Sensors Installation



Figure 6. STS Strain Transducer Installed on a Bridge Superstructure Member

3.2.2. STS Instrumentation and Testing Plan

Testing plans were made based on the critical path. Figure 7 shows an example of sensor location on the prestressed girder. The strain transducer were installed at top, mid-height and bottom.

Figure 8 presents the layout of strain transducers and accelerometer that were installed for this task. Twenty-Two (22) strain transducers and Six (6) accelerometers were installed along the girders. A summary of the total number of sensors is provided in Table 3. Figure 9 shows the installation of strain transducers and their corresponding BDI identification number.

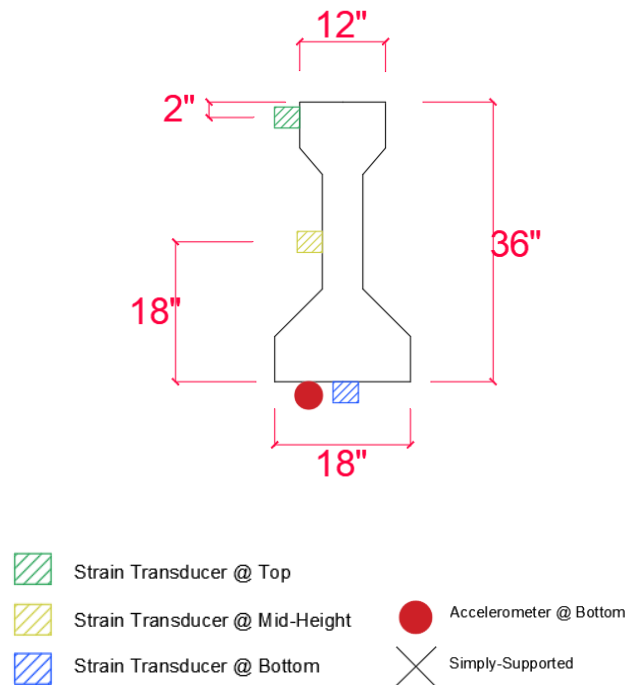


Figure 7. Typical Sensor Locations

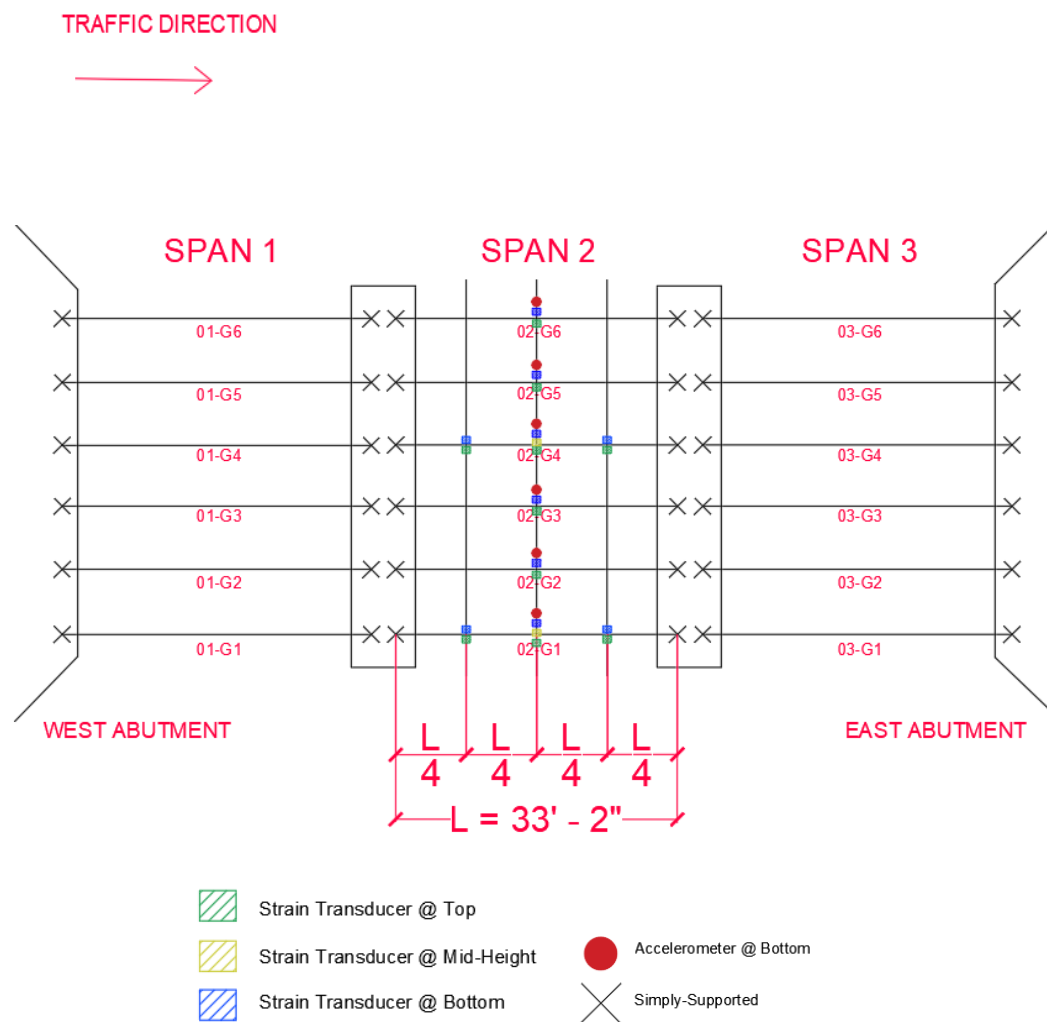


Figure 8. Layout of Sensors

Table 3. - Inventory of the Sensor Instrumentation underneath the Superstructure

Type of Sensor	Number of Sensors	Remark
Strain Transducers	22	Up to 4 x STS sensors per junction box.
Accelerometers	6	All junction boxes connect to a main unit.

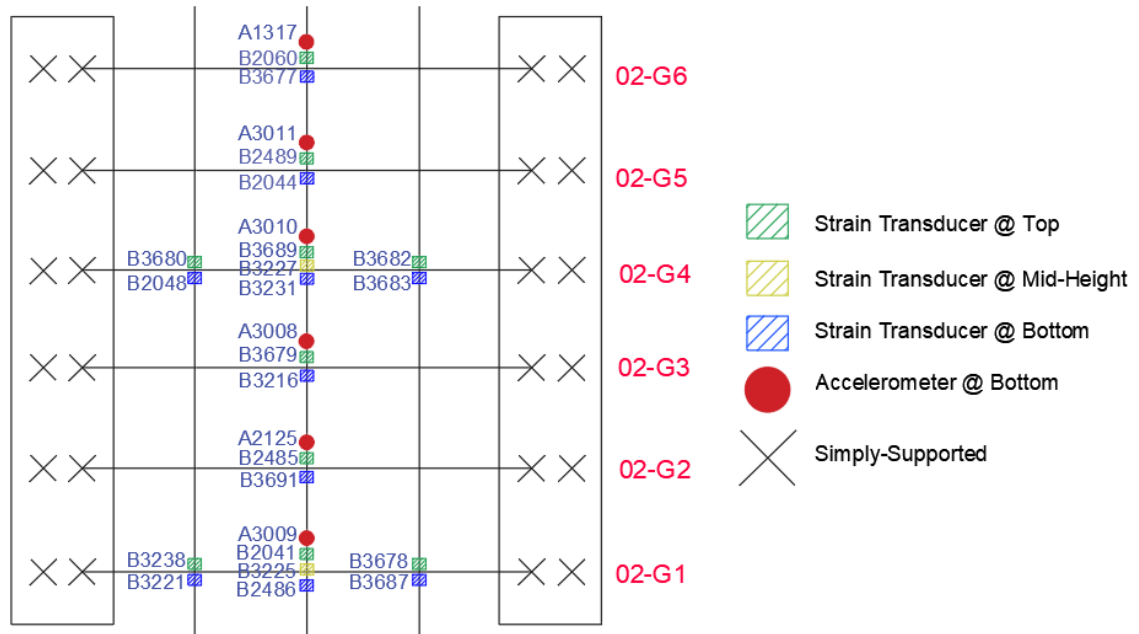


Figure 9. Strain Transducers Location and Number

3.2.3. Calibration Truck

A Class 6 Truck with 3-axle was utilized for a load test and the vehicle was loaded with a gross vehicle weight (GVW) of 54.7 kips. The aggregate was used to load the truck. Coarse aggregate was preferred rather than fine aggregate or sand for a stationary weight distribution. The weight certificates of each axle weight, as well as GVW, was provided by the truck driver prior to the performance of load test. Figure 10 explains the procedure to obtain the certificates of each axle or tandem and Figure 11 shows the actual calibration truck with axle weight,

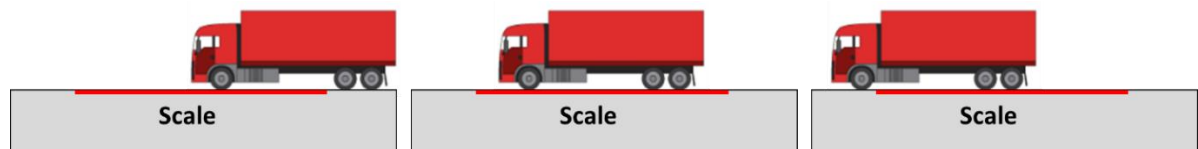


Figure 10. Weighing Procedure for Calibration Truck



Figure 11. Calibration Truck

3.2.4. Diagnostic Load Test

On November 20, 2017, the team went to install the sensors and test the strain sensor. Figure 12 shows the sensor installation. On November 21, 2017, the test was performed. Figure 13 shows the diagnostic load test on the target bridge. Figure 14 shows the paths of which truck ran across the bridge. Several load tests were performed at each load paths to ensure that the testing results are consistent and rational. The raw test results are shown in Figure 15. The vertical red lines were used to indicate the time when the truck entered and exited center span of the bridge. After the test was finished, the sensors were all removed.

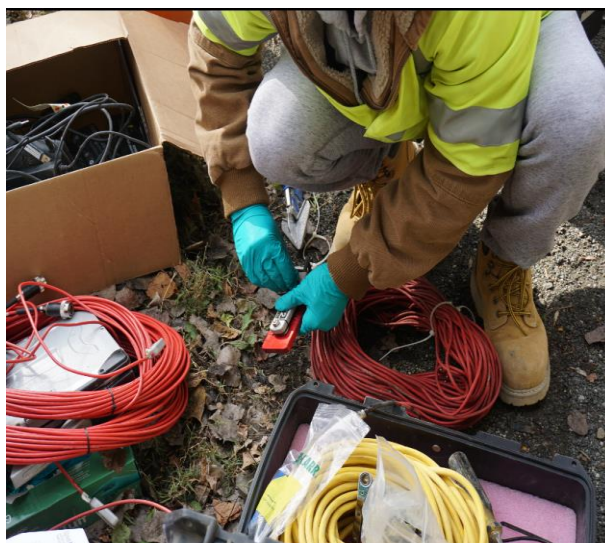


Figure 12. Sensor Installation



Figure 13. Diagnostic Load Test

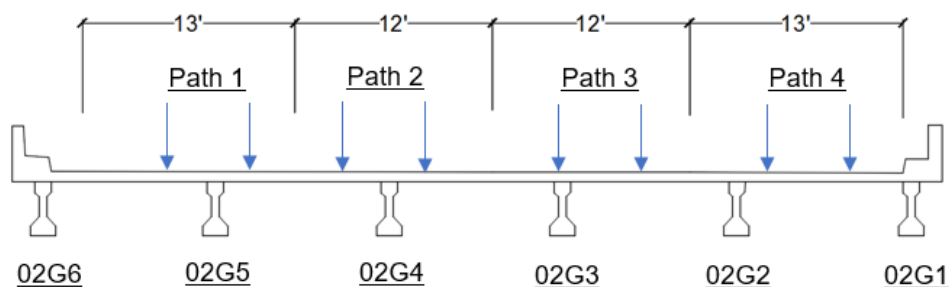


Figure 14. Diagnostic Load Paths

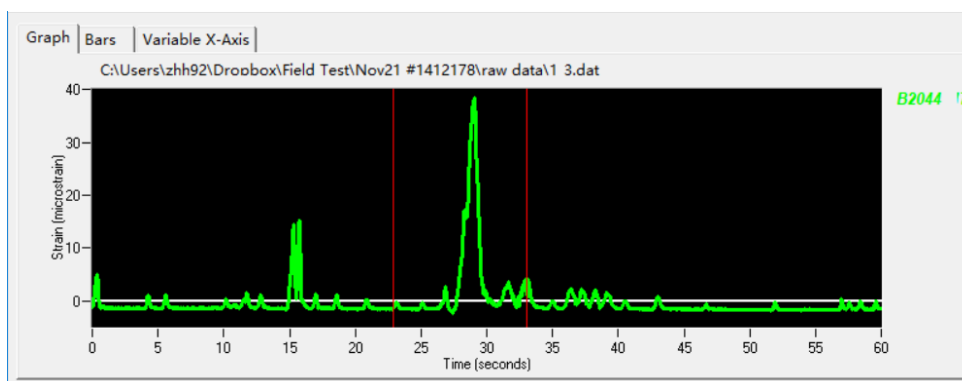


Figure 15. Raw Strain Data from BDI Software

3.2.5. Validation of Non-Destructive Test Tools

For NDT/E technique, various equipment including Schmidt Hammer, Windsor Probe, Ferroskan, and Profoscope have been used in the past studies to estimate the unknown parameters of the structure, such as concrete strength, the depth of concrete cover, rebar size, rebar corrosion, etc.

Among various NDT/E tools, the team selected two NDT/E tools that can estimate the concrete strength, cover depth, and rebar size and location, as shown in Figure 16. One is Schmidt Hammer and the other is rebar locator. Schmidt Hammer in Figure 16(a) provides the concrete strength of given element at a range between 1450 psi and 10152 psi. Figure 16(b) is the rebar locator or Profoscope+ for detecting the rebar and estimating the rebar size up to 2.5 in. (65 mm) and depth up to 7 in. (180 mm).



(a)



(b)

Figure 16. Proposed NDT/E tools for field testing; (a) Original Schmidt Hammer and (b) Profoscope+ (rebar locator)

The validation was done inside the Rutgers Infrastructure Monitoring and Evaluation (RIME) laboratory to establish the reliability and accuracy of the two NDT/E tools.

The rebar locator was tested on the beams with known rebar sizes and distribution. The results were also conservative in terms of the smaller estimated rebar size and the deeper concrete cover. It provided relatively reasonable information of rebar location and concrete cover at shallow depth and over non congested area, but the accuracy was not reliable as the concrete layer gets thicker and over a congested area.

The Schmidt Hammer was tested on the beams with different mixes and the concrete cylinders of those mixes were mechanical tested to confirm the strength. The results showed that the Schmidt Hammer provided lower compressive strength than that of actual strength. These are useful information as a guideline to ensure that the results getting from Schmidt Hammer are acceptable.

Table 4 summarizes the results of concrete compressive strength from Schmidt Hammer and compression machine. To get the reliable values of compressive strength from Schmidt Hammer, at least 10 to 12 impacts were performed on each test surface. As suggested by the manufacturer, Proceq, the corresponding dispersion was added to/subtracted from the average value in order to take into account of variation and accuracy of the equipment. Similarly, the average value from the compression machine was taken by taking an average of compressive strength from two (2) cylindrical concrete samples. These values are shown as the maximum and the minimum in Figure 17. And nine (9) more samples were tested to verify the results.

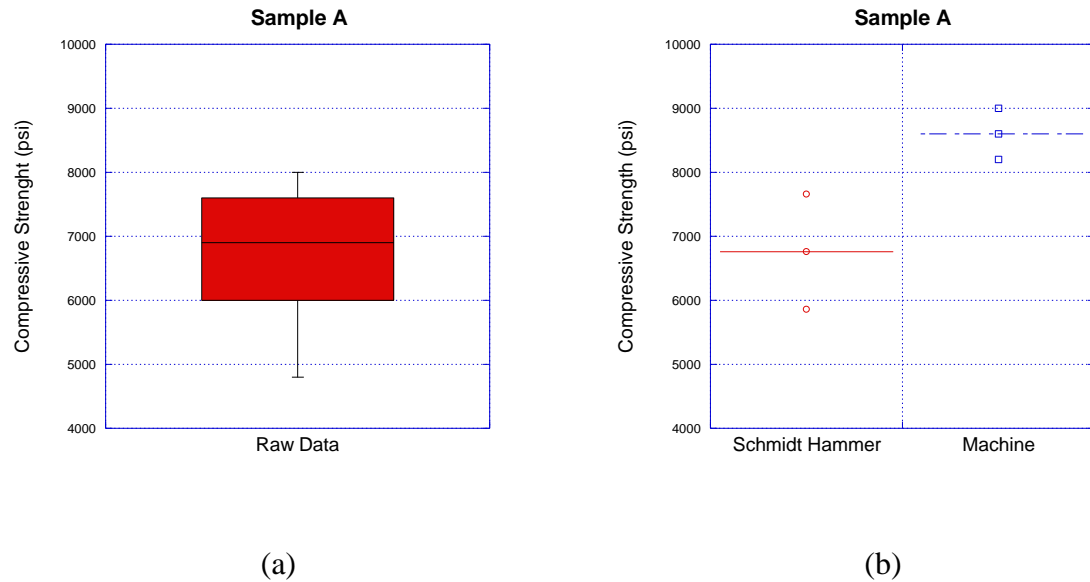


Figure 17. Sample A (a) Statistical Results (b) Comparison of Schmidt Hammer and Compression Machine.

The results show that the percentage difference between the estimated concrete compressive strength from Schmidt Hammer and the actual strength from the compression machine is range from 20.53% to 51.95% when comparing average value (Schmidt Hammer) to average value (machine). However, the percentage difference is lower, ranging from 9.08% to 34.61%, when comparing maximum (average + dispersion) value (Schmidt Hammer) to the average value (machine).

Based on the experimental results, the values of compressive strength from Schmidt Hammer are, nonetheless, conservative compared to the actual ones. Although the results from Schmidt Hammer are not 100% accurate, the result still shows there is at least a 5.72% conservation when the maximum value is used. To be conservative, the rating factors

shown in later section of this report are calculating based on the average compressive strength from the Schmidt Hammer.

Table 4. - Strength estimation of Schmidt Hammer

Sample	Actual Strength by Compressor Machine	Average Estimated Strength by Schmidt Hammer (% ratio compared to actual strength)	Average (+dispersion) Estimated Strength by Schmidt Hammer (% ratio compared to actual strength)
A	8600 psi	6760 psi (21.40 %)	7660 psi (10.93 %)
B	7520 psi	4905 psi (34.77 %)	5755 psi (23.47 %)
C	7424 psi	5900 psi (20.53 %)	6750 psi (9.08 %)
D	3165 psi	1521 psi (51.95 %)	2121 psi (32.99 %)
E	2793 psi	1750 psi (37.35 %)	2350 psi (15.87 %)
F	2976 psi	1875 psi (37.00%)	2525 psi (15.16 %)
G	2793 psi	1338 psi (52.09 %)	1938 psi (30.61%)
H	9037 psi	5775 psi (36.09 %)	6650 psi (26.41 %)
I	3933 psi	1892 psi (51.90 %)	2572 psi (34.61 %)
J	3328 psi	1696 psi (49.04 %)	2396 psi (28.01 %)

3.3. Test Results

Strain data for each run was stored, and MATLAB was used to perform data analysis and plot the strain versus time graphs for each sensor, as shown in Figure 18 through Figure 30

for critical path critical girder correspondingly and adjacent girders. To smooth the data, moving average was adopted to filter out the noise from the test. Within the period between the calibration truck entered and exited the center span, the most maximum strain (in microstrain) at bottom flange of the most critical girder was stored, along with corresponding time (in second). For instance, the most critical girder for Path 1 would be girder G5 and girder G4 for Path 2. The corresponding time of the most maximum strain was then used to obtain the strains from the other sensors.

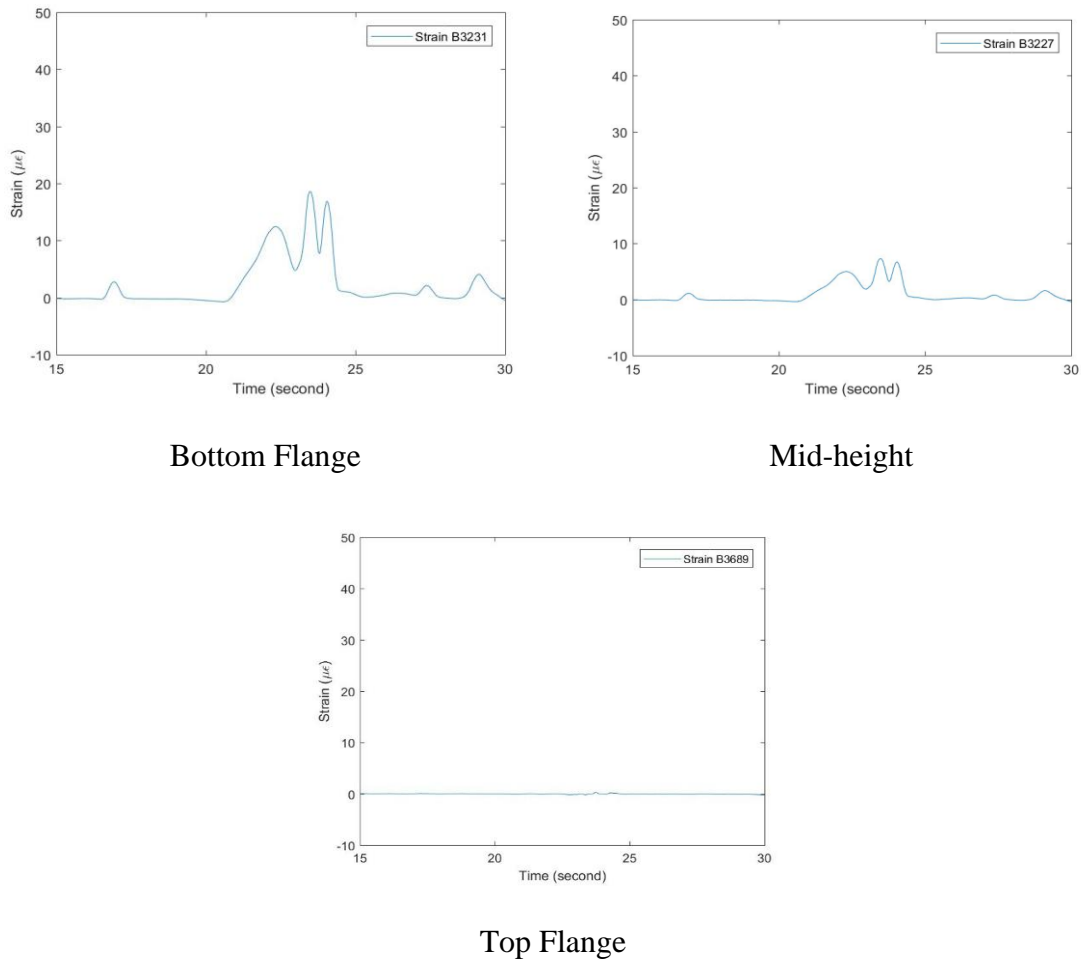
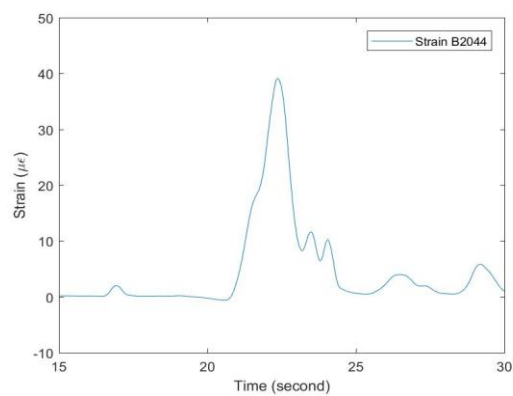
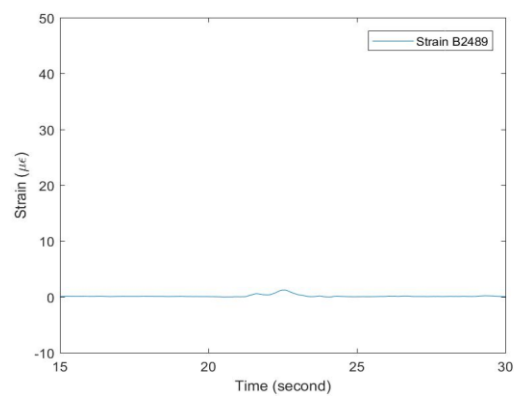


Figure 18. Measured Strain Data for PATH 1 / Girder G4

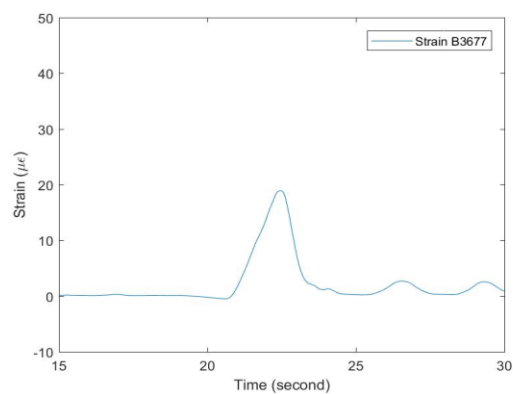


Bottom Flange

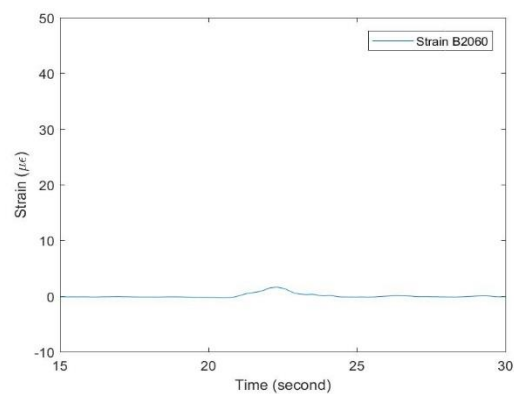


Top Flange

Figure 19. Measured Strain Data for PATH 1 / Girder G5

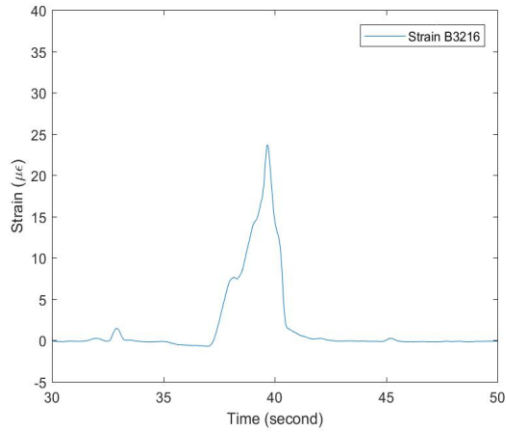


Bottom Flange

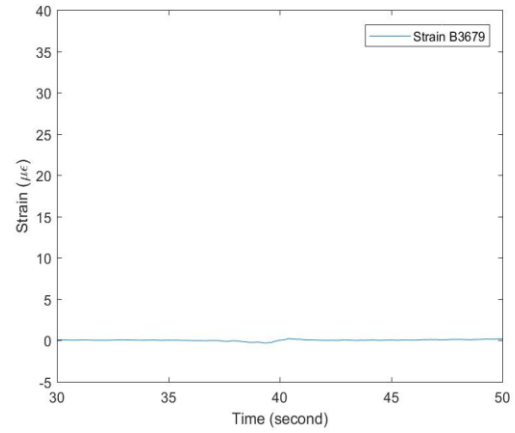


Top Flange

Figure 20. Measured Strain Data for PATH 1 / Girder G6

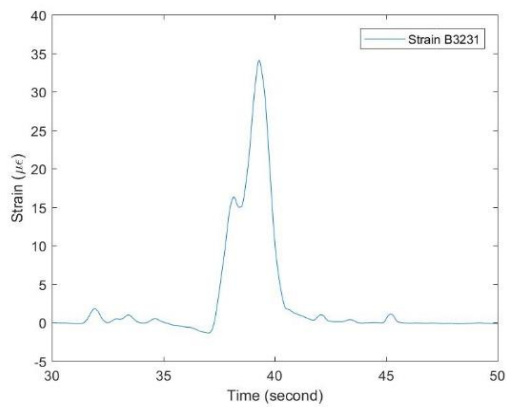


Bottom Flange

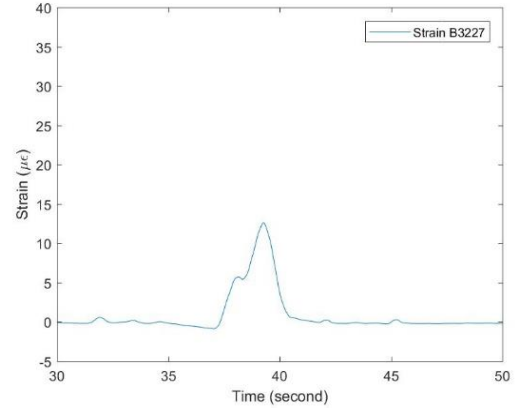


Top Flange

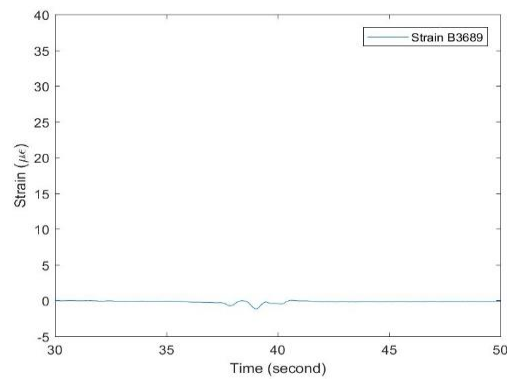
Figure 21. Measured Strain Data for PATH 2 / Girder G3



Bottom Flange

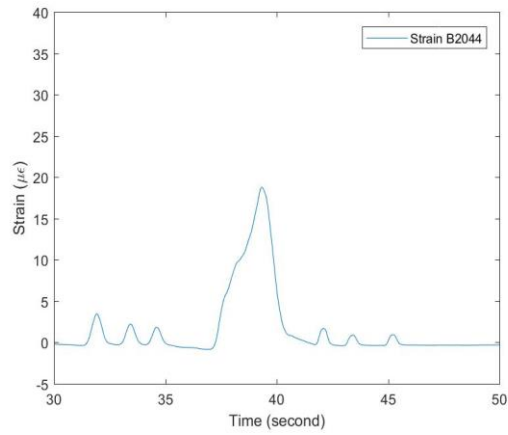


Mid-height

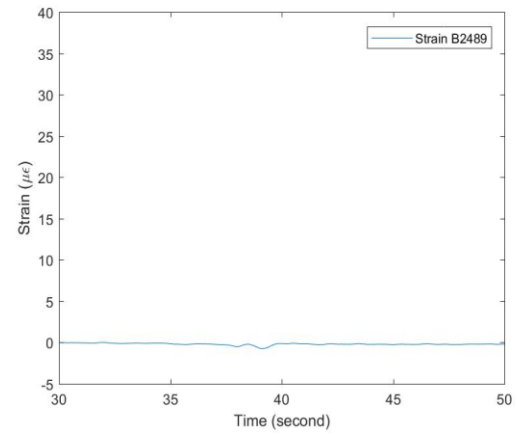


Top Flange

Figure 22. Measured Strain Data for PATH 2 / Girder G4

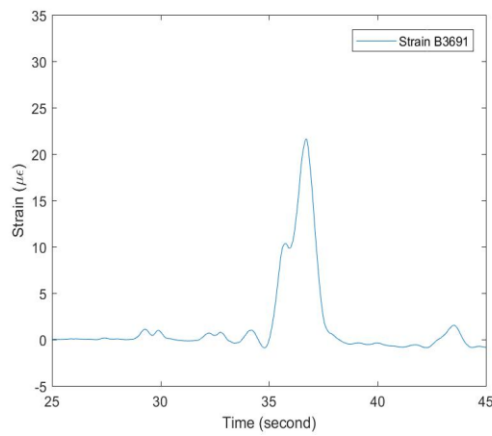


Bottom Flange

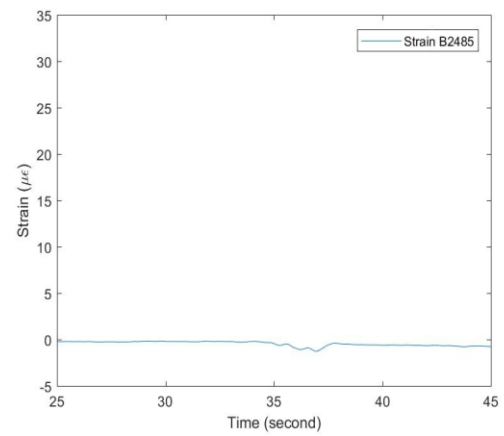


Top Flange

Figure 23. Measured Strain Data for PATH 2 / Girder G5

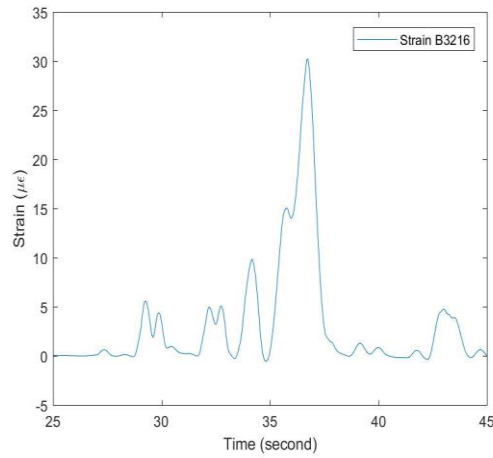


Bottom Flange

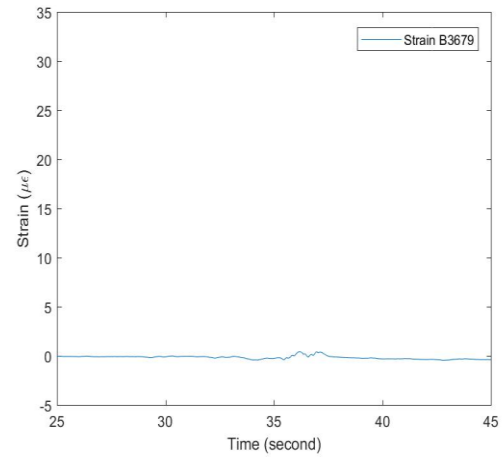


Top Flange

Figure 24. Measured Strain Data for PATH 3 / Girder G2

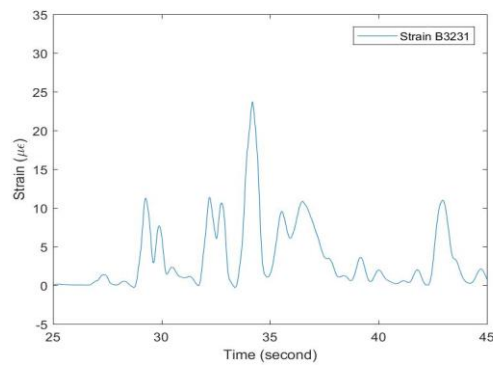


Bottom Flange

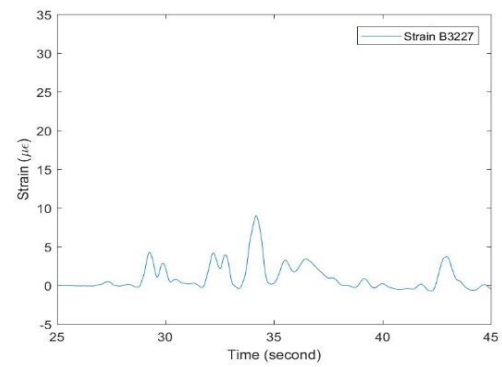


Top Flange

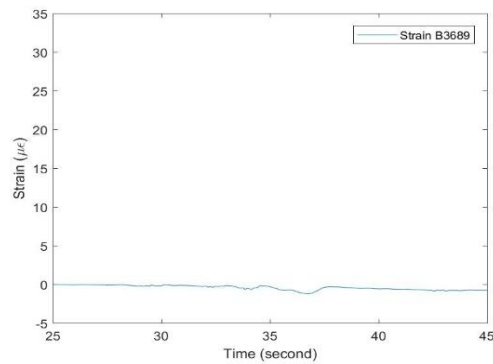
Figure 25. Measured Strain Data for PATH 3 / Girder G3



Bottom Flange

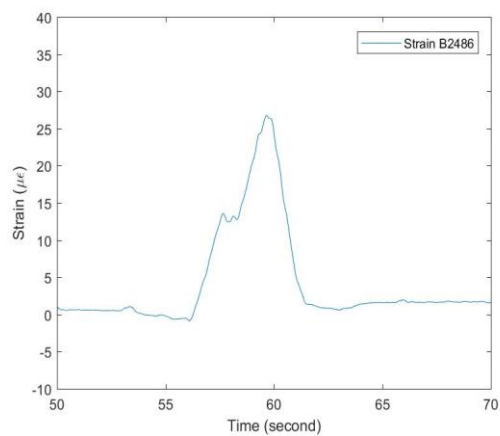


Mid-height

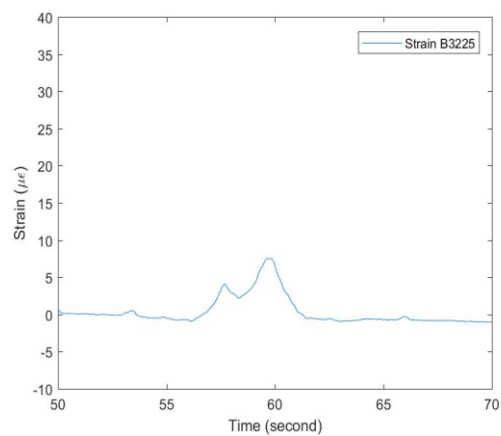


Top Flange

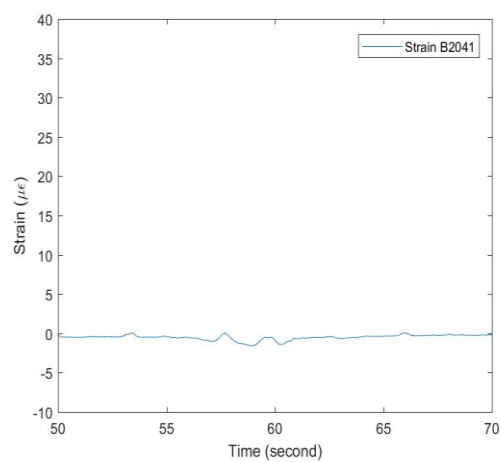
Figure 26. Measured Strain Data for PATH 3 / Girder G4



Bottom Flange

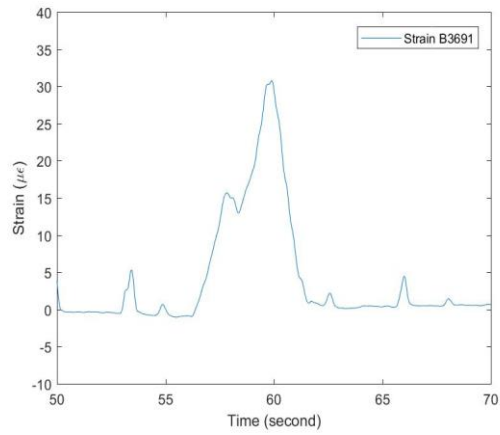


Mid-height

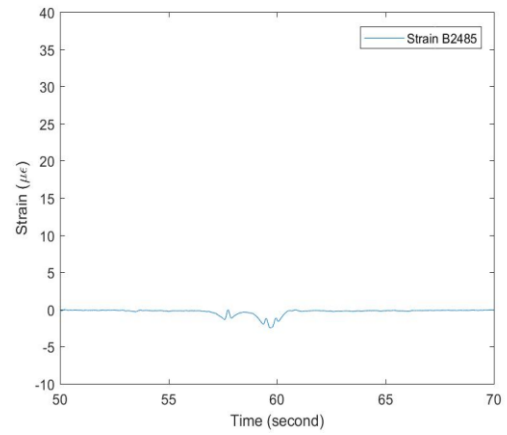


Top Flange

Figure 27. Measured Strain Data for PATH 4 / Girder G1

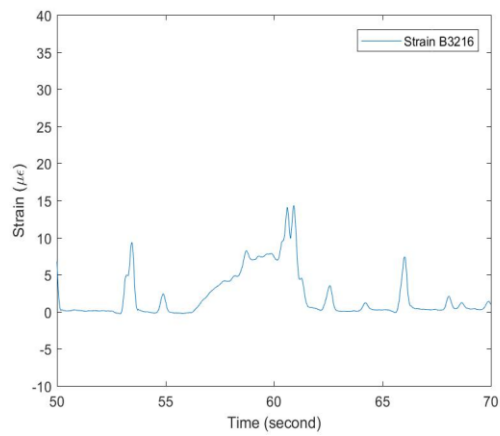


Bottom Flange

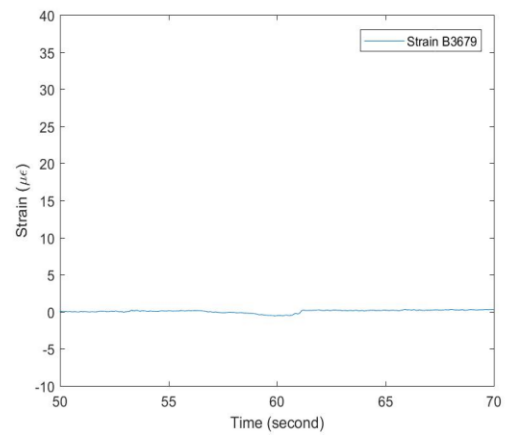


Top Flange

Figure 28. Measured Strain Data for PATH 4 / Girder G2

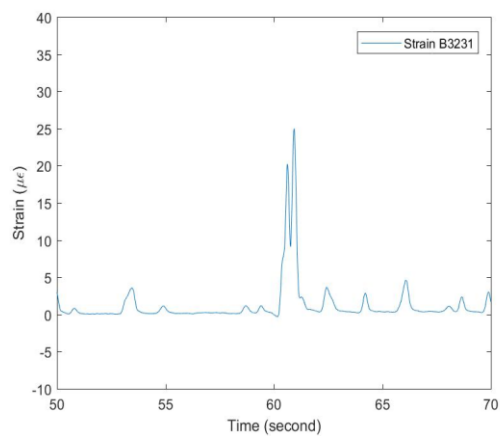


Bottom Flange

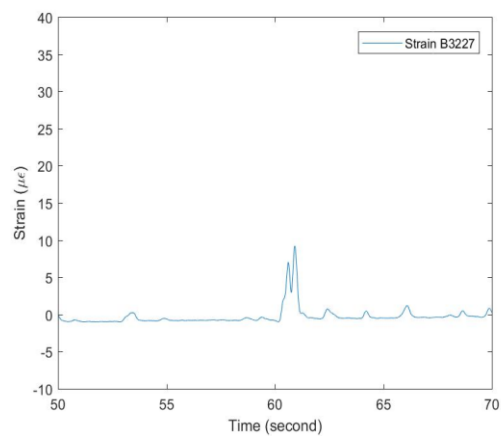


Top Flange

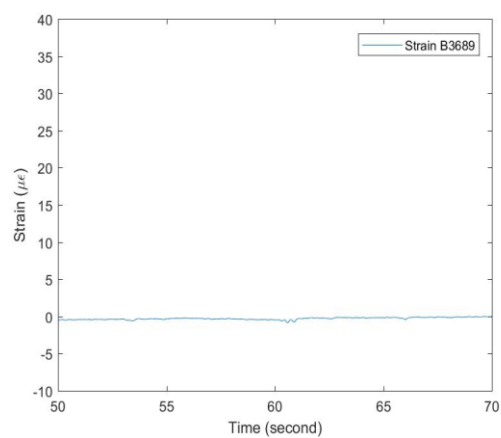
Figure 29. Measured Strain Data for PATH 4 / Girder G3



Bottom Flange



Mid-height



Top Flange

Figure 30. Measured Strain Data for PATH 4 / Girder G4

Chapter IV

4. Analysis of Bridges without Plans

4.1. Analysis of Bridges Known Plans

The bridges are first analysis for plans are available and set up a benchmark for analysis of bridges without plans. In this case, the bridge will be compared between as-built condition and condition of analysis the bridge as if there were no plans available.

4.1.1. Information Collection

For this study, a target bridge was selected for validating the procedure. The first step is to set up a benchmark for the testing bridge. Structure Number 1412-178 was selected for this study. The analysis of testing and load rating without plans was based on this structure.

From 17th cycle report of structure number 1412-178 [10], the cross-section of the girder is shown in Figure 31. And below are the assumptions of this analysis.

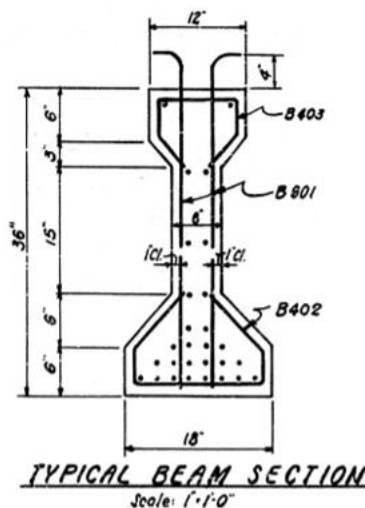


Figure 31. Cross-section of the Girder

(Source: Bridge Re-Evaluation Survey Report Structure No. 1412-178 17th cycle.)

- AASHTO type II is used for girder design
- Condition factor and system factor of the structure is 1.0
- Strand information
 - Strand tensile strength (f_{pu}) is 250 ksi
 - Twenty-eight (28) strands and diameter of 7/16" are used
 - The cross-section of the girder stays the same along the span length
 - the structure has two strands at the top layer, which in this case will contribute to compressive resistance at the top flange
 - Strands are also distributed in the web
 - No reinforcement rebar is shown from the plan
- Stirrup information
 - Stirrup tensile strength (F_y) is 40 ksi
 - Two stirrup legs (#6 bars)
 - Eighteen (18) spaced at 6"
 - Five (5) spaced at 9"
 - Two (2) spaced at 1'-0"
 - One (1) spaced at 1'-2" to the centerline

4.1.2. Validation of Load Rating Procedure

Based on AASHTO MBE [1], a spreadsheet is created used for calculating the load rating factor. To validate the spreadsheet, two rating examples are checked from MBE [1] and WisDOT Bridge Manual [7]. Because the philosophy of design and load rating is the same, important parameters can be compared for the validation purpose. Two design examples,

one example from PCI [8] and another one from Federal Highway Administration (FHWA) report [9]. The losses are calculated based on different method correspondingly.

Table 5. Rating Example 1 MBE

	Inventory (HL-93)	Operating (HL-93)	Shear RF	Service I Flexure	Strength II Flexure	Loss Estimate	Loss Refine
Our Design	1.48	1.92	1.96	1.23	1.69	20.98%	16.42%
MBE Design	1.48	1.92	1.96	1.22	1.69	21.10%	-

- Summary of Moments and shears				
	Support	Critical	Stirrup Change	Midspan
x/L	0	0.067	0.250	0.5
X	0.0	5.4	20.0	40
V_{DC1} , kips	75.85	65.68	37.93	-
V_{DC2} , kips	10.00	8.66	5.00	-
V_{DW} , kips	8.10	7.01	4.05	-
$g_m V_{LL+IM}$, kips	-	85.32	63.75	-
V_n , kips, MCFT	-	440.57	569.71	-
M_{DC1} , kip-ft	-	379.71	1137.78	1517.03
M_{DC2} , kip-ft	-	50.06	150.00	200.00
M_{DW} , kip-ft	-	40.55	121.50	162.00
$g_m M_{LL+IM}$, kips-ft	-	396.28	1155.74	1486.89
M_n , kip-ft	-	-	-	6245.19

Figure 32. Our Rating Spreadsheet Parameters

Location	Support	Critical Shear	Stirrup Change	Midspan
x/L	0.0	0.067	0.25	0.5
X , ft	0.0	5.37	20	40
V_{DC1} , kips	76	65.8	38	—
V_{DC2} , kips	10	8.7	5	—
V_{DW} , kips	8.12	7.03	4.1	—
$g_m V_{LL+IM}$, kips	—	85.3	63.7	—
V_n , kips, simplified	—	221.7	129.1	—
V_n , kips, MCFT	—	440.7	227	—
M_{DC1} , kip-ft	—	380.7	1140	1520
M_{DC2} , kip-ft	—	50.1	150	200
M_{DW} , kip-ft	—	40.7	121.8	162
$g_m M_{LL+IM}$, kip-ft	—	390.5	1087	1487.7
M_n , kip-ft	—	—	—	6244.4

Figure 33. MBE Rating Spreadsheet Parameters

Table 6. Rating Example 2 WisDOT Bridge Manual

	Inventory (HL-93)	Operating (HL-93)	Shear RF	Service III	Loss Estimate	Loss Refine
Our Design	1.729	2.241	1.96	1.49	19.52%	16.97%
MBE Design	1.723	2.233	1.96	1.43	19.54%	-

Table 7. Design Example 1 PCI

	# of Strands	Mu	Service III (Flexure)	Flexure Resistance	Loss (PCI)	Loss (Refined)
Our Design Spreadsheet	44	8590	0.290 (PCI Loss)	10699	19.54%	13.53% (Refined)
Their design	44	8590	0.290 (PCI Loss)	10697	19.59%	-

Table 8. Design Example 2 FHWA

	# of Strands	Mu	Service III	Flexure Resistance	Loss (PCI)	Loss (Refined)
Our Design Spreadsheet	48	9314	0.486 (Old Loss)	11364	26.39%	18.08%
Their design	48	9316	0.487 (Old Loss)	11364	26.40%	-

As can be seen from Table 5 to Table 8 above, the most important design and rating parameters are compared in the table. The parameters include the number of strands used, the strand pattern, the service III stress value, resistance value rating factor, and losses. All parameters are checked and have a difference for all parameters are within 1%.

4.1.3 Load Rating Bridges with Structure Number #1412-178

Based on developed spreadsheet and information from cycle report [10], the structure can be load rated for inventory and operation level at Strength I and Service III limit state. In this case, the calculation for Service III is based on live load factor equals to 1.0 and the refined losses calculation. For shear capacity, modified compression field theory is used. The results for different parameter and RFs are shown in Table 9 and Table 10.

Table 9 Summary of Moments and Shears (Given Plans)

	Support	Critical	Stirrup Change	Midspan
x/L	0	0.030	0.29	0.5
X	0.0	1.0	9.8	16.59
V_{DC1}, kips	36.77	34.56	15.16	-
V_{DC2}, kips	1.82	1.71	0.75	-
V_{DW}, kips	1.72	1.62	0.71	-
$g_m V_{LL+IM}, \text{kips}$	-	77.13	47.04	-
$V_n, \text{kips}, \text{MCFT}$	-	475.65	315.10	-
$M_{DC1}, \text{kip-ft}$	-	35.67	253.16	304.95
$M_{DC2}, \text{kip-ft}$	-	1.77	12.56	15.13
$M_{DW}, \text{kip-ft}$	-	1.67	11.87	14.30
$g_m M_{LL+IM}, \text{kip-ft}$	-	75.14	462.91	495.74
$M_n, \text{kip-ft}$	-	-	-	2121.14

Table 10. Rating Factor for Bridge Structure #1412-178 Based on Given Plans

Limit state	HL-93	
	Inventory RF	Operating RF
Strength I	-	-
Flexure(at midspan)	1.96	2.54
Shear(at critical)	2.82	3.65
Shear(at change)	3.19	4.14
Service III	-	-
Flexure(at midspan)	1.39	-

4.2. Results from Testing Data

From the diagnostic load test and NDT/E, actual structural behavior can be observed. It is important for the engineers to understand the actual response, because the variances during construction and service, which might have changed the structural behavior. For example, some unintentional composited action might increase the rigidity, some cracks leading to change in load distribution, etc. Furthermore, from testing, information can be updated to the analytical model when analyzing a bridge without plans.

4.2.1 NDT/E Results

NDT/E tools, Schmidt Hammer and GPR, were performed by AID. Inc. The results were used for updating rating factors and structure analysis.

The GPR was used for measuring the stirrup spacing. The GPR results are shown in Figure 34. The inverted hyperbola represents the rebar perpendicular to the direction of testing. From testing, the rebar spacing is estimated of 0.3-0.8 ft and depth of 1.5-1.8 in.

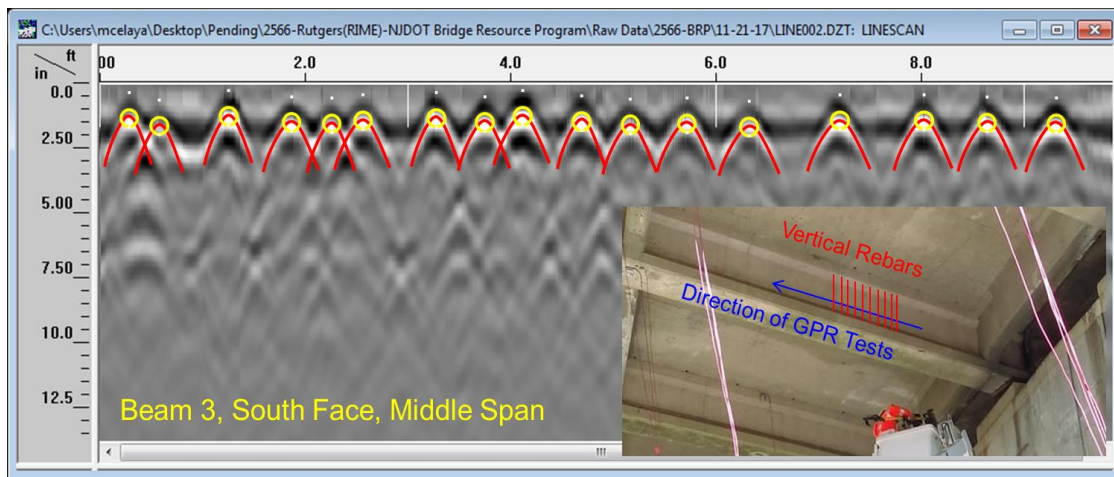


Figure 34 GPR Results (Photo provided by AID Inc.)

The Schmidt Hammer was used for estimating the concrete compressive strength (f'_c), from testing the strength is 7.4 ksi. Ten (10) locations were chosen and perform the test, shown in Figure 35.

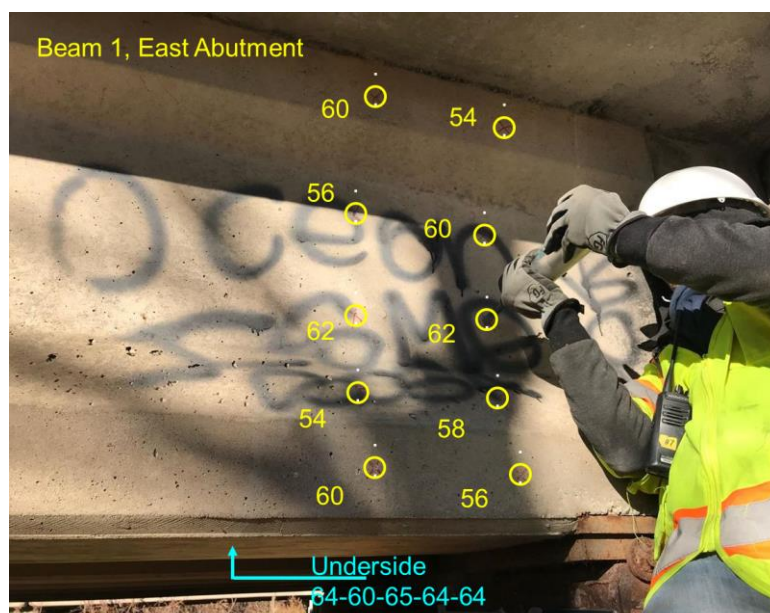


Figure 35. Schmidt Hammer Testing (Photo provided by AID Inc.)

4.2.2 Neutral Axis Analysis

With known strains and sensor locations on the girder, the neutral axis of the prestressed girders for each run was then calculated in Table 11. These experimental neutral axis values are compared with the theoretic value. Because of the variance, the only value in red color with less noise impacted can be used for analysis.

Table 11. Neutral Axis (from bottom flange) Data with the Corresponding Path

Path	Run	G1	G2	G3	G4	G5	G6
	1	27.86	23.66	35.60	33.02	34.85	37.04
	2	28.02	277.48	26.96	31.73	34.34	37.09
	3	135.65	2.31	35.28	34.04	35.23	37.80
	4	24.90	0.34	36.64	34.56	35.19	38.26

2	1	18.35	29.18	33.37	32.23	32.80	41.54
	2	16.73	34.96	33.39	32.36	32.81	43.04
	3	19.69	30.75	33.44	32.01	32.12	37.77
	4	12.49	31.67	32.74	32.10	32.94	31.41
3	1	55.82	32.40	34.14	28.94	30.88	40.56
	2	29.38	32.20	32.85	28.30	22.99	74.38
4	1	30.65	32.47	31.62	9.37	26.29	18.85
	2	32.15	31.87	30.31	28.43	32.88	-8.17

For interior girder, the neutral axis in the elastic range is 30.43'' (the strands are included) and 30.23'' (the strands are not included) from the bottom layer. For exterior girder, the neutral axis is 29.61'' (the strands are included) and 29.38'' (the strands are not included) from the bottom layer. Comparing the calculation with experimental results from the table, the reasons that cause the differences are likely to be the following:

1. The actual compressive strength of the girder and deck

From cycle report, the compressive strength (f'_c) is 3 ksi for the deck and 5 ksi for the girder. In reality, the concrete however might reach to a larger value. The Schmidt Hammer test gave a value of 7.4 ksi for the compressive strength of the girders.

2. Effective transformed flange width

The effective width, in reality, could be larger than the value used in AASHTO LRFD Specifications equations [11].

For interior girders, the effective flange width is the least of

- a. One-quarter of the average span length
- b. Twelve times the average thickness of the slab, plus the greater of the web thickness or one-half the width of the top flange of the girder
- c. The average spacing of adjacent girders

For exterior girders, the effective flange width is one-half the effective flange width of the adjacent interior girder, plus the least of

- a. One-eighth of the effective span length
- b. Six times the average thickness of the slab, plus the greater of one-half of the web thickness or one-quarter of the width of the top flange of the girder
- c. The width of the overhang

3. Deterioration and crack at the bottom flange

Since the bridge was built in 1959 and it might have seen some heavy load during service life which cracked the girders.

A sensitivity analysis was performed based on strand number. Theoretically speaking, the neutral axis varies from different strand pattern. If the neutral axis can be calculated from the test, the pattern can be estimated. However, when computing the neutral axis in the elastic range, because of strain compatibility, the tension is taken mostly by the concrete. From the study, it is found that the neutral axis is not sensitive to the strand number.

4.2.3 Strain Results Comparison and Girder Distribution Factor (GDF)

Hag-Elsafi (2006) performed a load test and analysis the testing results. By using the strains obtained from load test, the GDFs can then be calculated using the equation based on strain distribution [12]. GDF for one-lane loaded was calculated based on equation (8)

$$GDF = \frac{\text{Strain (bottom flange) of One Girder At Midspan}}{\text{Total Strain (bottom flange) At Midspan}} \quad (8)$$

GDF for two-lanes and three-lanes loaded was calculated by using superposition method. To be conservative, the GDF was selected based on maximum value, for both interior and exterior girder. For an interior girder, the GDF was 0.658, based on the strain from girder G5. For an exterior girder, the GDF was 0.492 based on the strain from girder G1. These actual GDFs are then compared with GDFs calculated using AASHTO LRFD Specifications [11]. From AASHTO equations, the GDFs are 0.741 and 0.68 (using lever rule) for the interior and exterior girder, respectively. For two-lane loading, the GDF of interior is 0.803 from test (0.986 from AASHTO) and exterior is 0.393 (0.548 from AASHTO). Based on this study, it shows that the AASTHO LRFD Specifications provides the conservative values for GDFs.

Based on the strain results at the bottom flange, the GDF of each girder can be calculated. Table 12 shows the summary of the GDF from testing. The red and the blue color denote the maximum GDF of interior and exterior girder, respectively.

Table 12. - Distribution Factors Based on Load Test

Path	Run	G1	G2	G3	G4	G5	G6
1	1	-0.009	-0.007	0.032	0.175	0.548	0.262
	2	-0.006	-0.004	0.026	0.154	0.536	0.294
	3	-0.006	-0.001	0.028	0.173	0.543	0.263
	4	-0.010	0.000	0.036	0.179	0.537	0.257
2	1	-0.016	0.048	0.216	0.470	0.258	0.025
	2	-0.005	0.063	0.222	0.448	0.251	0.022
	3	-0.010	0.045	0.215	0.465	0.262	0.024
	4	-0.008	0.037	0.198	0.456	0.278	0.039
3	1	0.034	0.313	0.438	0.144	0.058	0.014
	2	0.041	0.328	0.483	0.136	0.023	-0.011
4	1	0.410	0.483	0.123	0.003	-0.016	-0.002
	2	0.301	0.398	0.147	0.084	0.072	-0.002

Table 13 summarizes the GDFs of one-lane, two-lane, and three-lane load for both interior and exterior girder. It should be noted the multiple presence factors are already included in the values shown in Table 13.

Table 13. - Summary of Maximum GDFs

	Interior	Exterior
One-lane loaded	0.658	0.492
Two-lanes loaded	0.803	0.393
Three-lanes loaded	0.717	0.327
Govern	<u>0.803</u>	<u>0.492</u>

Furthermore, the following Equation (9), (10), and (11) from AASHTO LRFD Specifications [11] are used to calculate moment GDFs. As shown in Table 14, by comparing the results from AASHTO equations to those from the load test, it is found that the AASHTO specification uses more conservative values.

Moment Distribution for Interior Beams

One Lane Loaded:

$$g = 0.06 + \left(\frac{S}{14}\right)^{0.4} \left(\frac{S}{L}\right)^{0.3} \left(\frac{K_g}{12.0L_s^3}\right)^{0.1} \quad (9)$$

Two or More Lanes Loaded:

$$g = 0.075 + \left(\frac{S}{9.5}\right)^{0.6} \left(\frac{S}{L}\right)^{0.2} \left(\frac{K_g}{12.0L_s^3}\right)^{0.1} \quad (10)$$

where

g = distribution factor

S = spacing of beams (ft.)

L = span of beam (ft.)

K_g = longitudinal stiffness parameter (in⁴)

T_s = depth of concrete slab (in.)

Moment Distribution for Exterior Beams

One Lane Loaded: Lever Rule

Two or More Lanes Loaded:

$$g = e g_{\text{interior}}$$

$$e = 0.77 + \frac{d_e}{9.1} \quad (11)$$

where

g_{interior} = distribution factor of interior girder

e = correction factor

d_e = distance from the exterior web of the exterior beam to the interior edge of curb
or traffic barrier (ft.)

Table 14. - Calculated GDFs Using AASHTO Specification [11]

	Interior	Exterior
One-lane loaded	0.741	0.581
Two or more lanes loaded	0.986	0.710
Govern	<u>0.986</u>	<u>0.710</u>

4.2.4 Load Effect and Posting Load

Comparing the load effects generated by the calibration truck and legal truck load model. Based on the calculation, the load effect of a Class 6 Truck is greater than those of legal loads. The comparison of load effect between Legal load and calibration truck is shown in Table 15. It shows that the moment effect and shear effect caused by this truck is slightly larger than the legal truck.

Table 15. - Load effect comparison between Legal load and calibration truck

Truck Type	Weight (Kips)	Shear Effect (Kips)	Moment Effect (Kip-ft)
Calibration Truck	54.7	40.0	268.5
Type 3 Unit	50.0	38.4	263.7
Type 3-3 Unit	80.0	32.1	213.7
Type 3S2 Unit	72.0	34.4	252.8

The strain was calculated based on truck configuration and GDFs from AASHTO Specification [11]. Using equation (34), the calculated strain was 48.7 micro-strain. From the load test, one of the strain transducers observed the largest strain of 42 micro-strain, which is reasonable and slightly smaller than the calculation. Because in reality, the stiffness might be higher, and the truck might not be exactly on top of the girder. Also, the strain is less than 300 microstrain, so the truck does not make any damage to the bridge.

$$\varepsilon = \frac{My}{EI} \quad (34)$$

ε = Strain

M_y = Moment \times Distance from the centroid to bottom fiber

EI = Bending stiffness

4.3. Analysis of Bridges without Plans

The preliminary “Guideline for Load Rating Assessment of Bridges without Plans” is shown in Figure 36. Beyond NDT/E methods, the Finite-Element Models are needed to refine the rating factors.

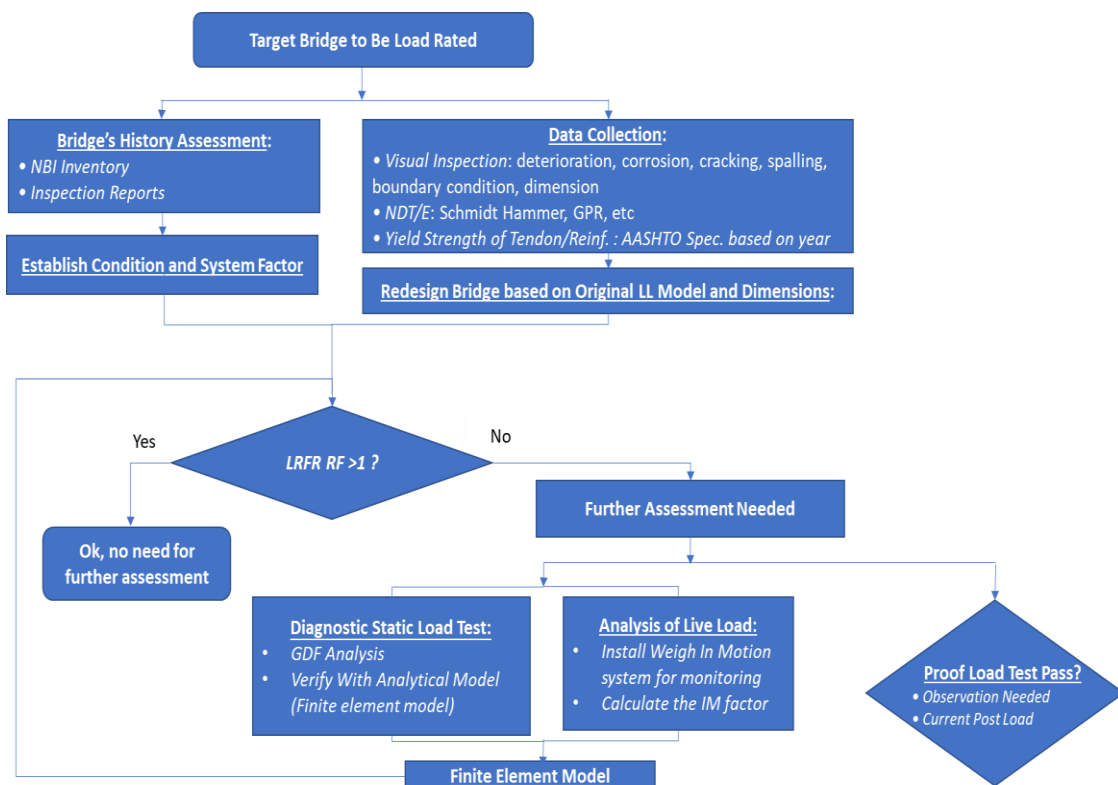


Figure 36. Guideline for Load Rating Assessment of Bridges without Plans

4.3.1. Re-design of the Bridges

Naaman (1982) stated that the design of a P/C member is governed by limiting the stresses that may cause the materials to fail under combined external and internal forces [13]. Four stress inequality conditions must be satisfied, where the actual stress must be less than the code allowable stress. These conditions control the service limit state for P/S bridges and they have been used for designing P/C since the beginning. Table 16 shows the four conditions.

Condition	Stress Inequality Equations
I	$1/F_i \leq (e_0 - k_b) / (M_{\min} - \overline{\sigma}_{ci} Z_t)$
II	$1/F_i \leq (e_0 - k_t) / (M_{\min} + \overline{\sigma}_{ti} Z_b)$
III	$1/(F \text{ or } \eta F_i) \geq (e_0 - k_b) / (M_{\max} - \overline{\sigma}_{is} Z_t)$
IV	$1/(F \text{ or } \eta F_i) \geq (e_0 - k_t) / (M_{\max} + \overline{\sigma}_{cs} Z_b)$
V	$e_0 \leq (e_0)_{mp} = y_b - (d_c)_{\min} = \text{maximum practical eccentricity}$

Table 16. Four Stress Inequality Equations

Condition I stands for the stresses at transfer stage under minimum loading at top less than tensile limit stresses. Condition II stands for the stresses transfer stage under minimum loading at bottom less than compression limit stresses. Condition III stands for the stresses at service stage under maximum loading at top less than compression limit stresses. Condition IV stands for the stresses at service stage under maximum loading at bottom less than tensile limit stresses. Condition V stands for the practical condition.

To re-design the bridge, a graphical interpretation of the four stress conditions is used for this study named Magnel Diagram, Naaman (1982) also named it as feasibility domain. To keep consistent, this study also use the name of feasibility domain. The four inequality conditions create a bounded region which gives an infinite number of solutions. Figure 37 shows the graphical interpretation. The x-axis represents the inverse of the prestressing force. The Y-axis represents the eccentricity of strands. Essentially, every point in the shaded region can be used as a design point.

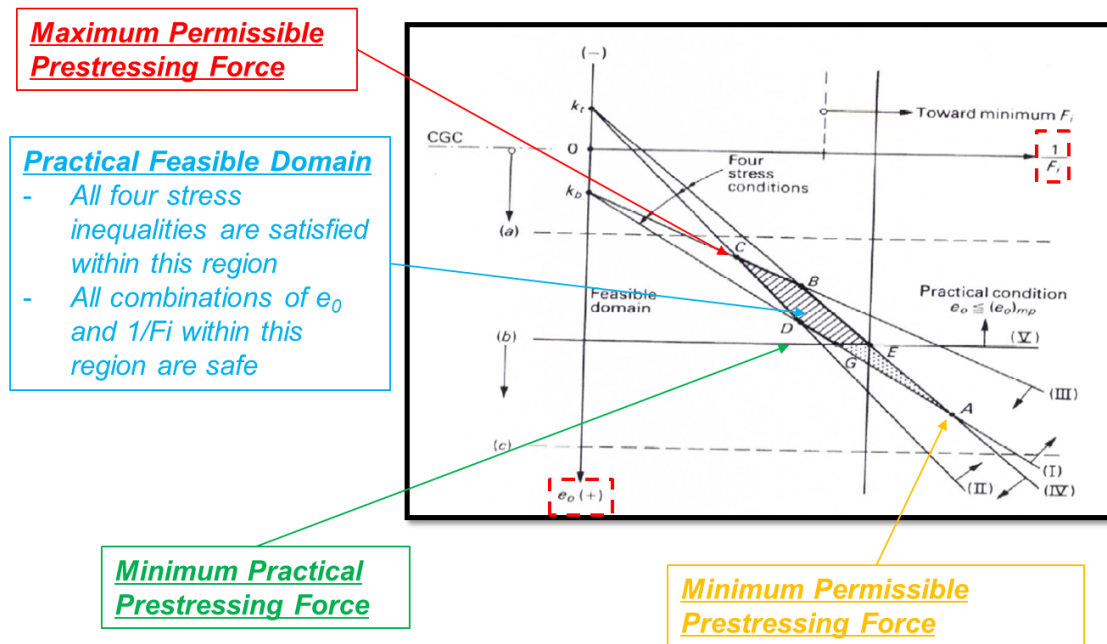


Figure 37. Feasibility Domain

(Source: *Prestressed Concrete Analysis and Design Fundamentals 2nd Ed* [13])

Based on the design live load model, HS-20, using feasibility domain analysis, the theoretical results of strands number can vary from 18 to 40, as shown in Figure 38. The maximum number of tendon, minimum required tendon and as-built design point are labeled in the feasibility domain graph. For the practical purpose, iterations were performed

to satisfy the eccentricity condition. Forty (40) strands were not used, although forty strands can satisfy the stress condition, the eccentricity based on practice will be 2.23. From feasibility domain, this maximum permissible point is not acceptable due to the large eccentricity. Thirty-six (36) strands were selected for the maximum design. For all the cases, several tendons are distributed at the top because the bottom fiber might exceed the compression limit at transfer stage. Eighteen (18) strands were selected for the minimum design. The layout is shown in Figure 39. With the feasibility domain, a losses percentage need to be assumed at first. The stresses need to be checked in the stresses inequality equation with the losses calculated based on selected tendon number.

When load rating the shear capacity of the bridge, the stirrup spacing can be estimated by the GPR. The results from GPR showed that the rebar spacing is about 0.3-0.8 ft and depth about 1.5-1.8 inches. In this case, the rebar spacing is compared with the as-built plan, which is #6 size rebar spacing at 0.5 ft. However, GPR is not able to provide the rebar size. Size #4 rebar spacing at 6 inches is assumed for further calculation. The design profiles that were estimated based on the feasibility domain are defined as “re-design” in this report.

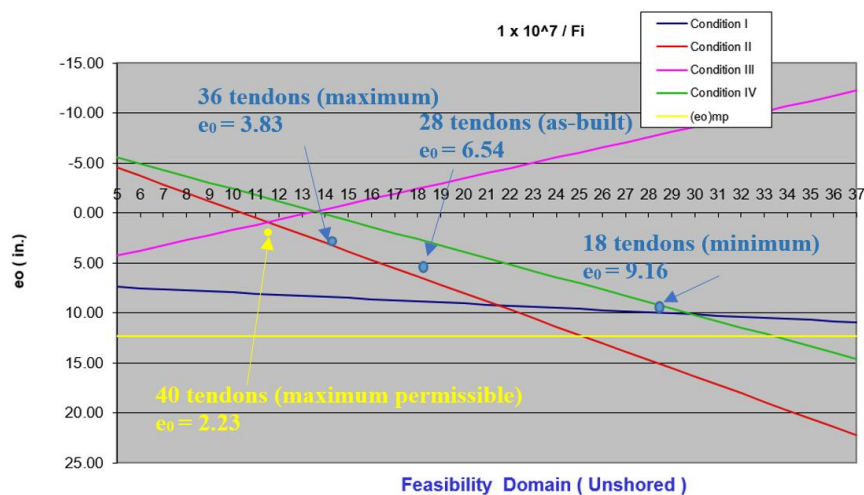


Figure 38. Feasibility Domain for HS-20



Figure 39. New Design Section

Then the Design Load (HL-93) rating factors based on AASHTO MBE [1] of the “re-design” structure are calculated and shown in Table 17. Also, the capacity is updated with compressive strength collected from Schmidt Hammer. From the results, the compressive strength only helps increase the flexure capacity by 3.2%. However, for shear and stress limit, compressive strength help increase the rating factor by 20.0% and 22.0%

Table 17. - Rating Factor for Re-design (re-design with 18 tendons)

Limit state	HL-93	
	Inventory RF	Operating RF
Strength I	-	-
Flexure (at midspan)	1.26	1.63
Flexure (at midspan)*	1.30	1.68
Shear (at critical)	1.40	1.81
Shear (at critical)*	1.68	2.19

Service III	-	-
Flexure (at midspan)	0.967	-
Flexure (at midspan)*	1.18	-

* With Schmidt Hammer

The flexure capacity is 1515.06 kip-ft. For shear, size #4 rebar (in pair) stirrup spacing at 6 inches are used at the support. The shear resistance is 271.87 kips. A summary of moments and shears is shown in Table 18. A rating factor summary for maximum strands is shown in Table 19. From Table 17 and Table 18, the updated compressive strength from Schmidt Hammer increased the resistance in service limit state flexure and shear.

Table 18. - Summary of Moments and Shears (re-design)

	Support	Critical	Midspan
x/L	0	0.091	0.5
X	0.0	3.0	16.59
V _{DC1} ,kips	36.77	30.07	-
V _{DC2} ,kips	1.82	1.49	-
V _{DW} ,kips	1.91	1.56	-
g _m V _{LL+IM} ,kips	-	68.82	-
V _n ,kips,MCFT	-	233.36 (271.87*)	-

M_{DC1} ,kip-ft	-	101.12	304.95
M_{DC2} ,kip-ft	-	5.02	15.13
M_{DW} ,kip-ft	-	5.24	15.82
$g_m M_{LL+IM}$,kip-ft	-	207.96	495.74
M_n ,kip-ft	-	-	1515.06 (1542.82*)

* With Schmidt Hammer

Table 19. Rating Factor for Re-design (re-design with 36 tendons)

Limit state	HL-93	
	Inventory RF	Operating RF
Strength I	-	-
Flexure (at midspan)	2.32	3.01
Shear (at critical)	1.08	1.40
Service III	-	-
Flexure (at midspan)	1.35	-

A sensitivity study was performed to apply the feasibility domain to the structure and the results, as shown in Table 20. Any tendon and eccentricity combination within the range from 18 to 36 is a possible solution.

Table 20. - Sensitivity Study Summary

No. of tendon	Tendon Eccentricity	Flexure Capacity (kip-ft)	Stirrup at support	Shear capacity
18	9.16	1515.06 (2 tendon on top)	Two #5 @ 6 in	339.39 (0 harped)
20	9.23	1677.82 (2 tendon on top)	Two #5 @ 6 in	349.96 (0 harped)
22	9.28	1838.34 (2 tendon on top)	Two #5 @ 6 in	361.00 (0 harped)
24	9.16	1988.74 (2 tendon on top)	Two #5 @ 6 in	327.55 (2 harped)
26	7.06	2012.72 (4 tendon on top)	Two #5 @ 5 in	373.66 (2 harped)
28	6.69	2130.77 (4 tendon on top)	Two #5 @ 5 in	346.85 (6 harped)
30	5.30	2170.21 (6 tendon on top)	Two #6 @ 6 in	372.20 (4 harped)
32	4.33	2228.42 (8 tendon on top)	Two #6 @ 6 in	378.39 (4 harped)

For reference, instead of as-built design load, HS-20, the author also performed feasibility domain on same structure based on the current design live load model HL-93, with a live load factor of 1.0. From feasibility domain shown in Figure 40, the strand number has a range from 20 to 39. The flexure capacity for 20 strands is 1677.8 kip-ft. Design using different live load model, the results show a discrepancy, but the difference is not large. For a heavier live load model, two (2) more tendons are needed to prevent the tension crack at the bottom. Thus, using the old design live load, HS-20, would be more critical for load rating and more similar to the as-built situation. For future results, the authors only use as-built design load to determine the feasibility domain of structure.

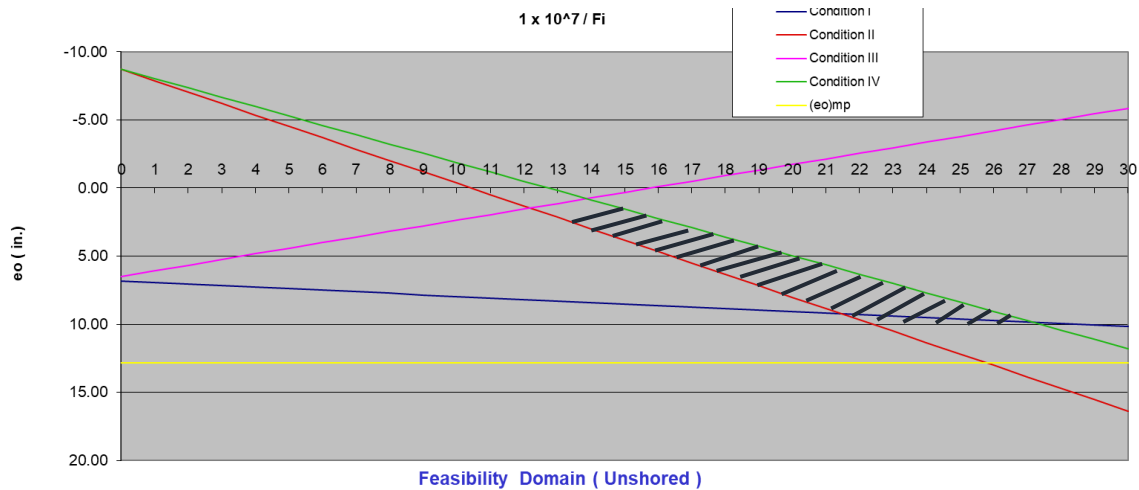


Figure 40. Feasibility Domain for HL-93

For flexure, the minimum design is the least tendons which satisfied the feasibility domain. Compare the flexure resistance of as-built design with feasibility results for HS-20, the flexure resistance of as-built bridge has a 39.9% more capacity than the minimum design. Compare the flexure resistance of as-built design with feasibility results for HL-93, the flexure resistance of as-built bridge has a 26.4% more capacity than the minimum design.

For shear capacity, the minimum design is calculated based on GPR and the assumption that #4 size stirrups are used for shear resistance where the as-built bridge is using #6 with six (6) inch spacing. The as-built bridge has an 82.7% more capacity than the minimum design. Furthermore, with Schmidt Hammer updating the compressive strength, comparing to 82.7%, the as-built bridge has a 56.7% more capacity than the minimum design. The data shows that the compressive strength help increase the estimation of shear resistance of the 26%. Also, the size of stirrup is an important variable for load rating the shear capacity while it cannot be measured using NDT/E tool. For reference, using assumption

of #5 stirrup for minimum design, the as-built bridge has a 25.7% more capacity than the minimum design. And with measured compressive strength, the estimated shear resistance has an 8.7% than minimum shear capacity, which is relatively close. From the data collecting within the same era, with engineering judgment, stirrup size can be decided conservatively.

4.4. Comparison of Load rating Results

Based on re-design calculation, the rating factors of the bridge are calculated. Table 21 shows the summary of rating factor for Bridge #1412-178, calculated based on the information from 5 different scenarios 1) as-built design (28 tendons), 2) similar to scenario 1 utilizing concrete compressive strength from Schmidt Hammer, 3) the bridge is redesigned with minimum requirement of tendons (18tendons), 4) similar to scenario 3 utilizing concrete compressive strength from Schmidt Hammer, and 5) similar to scenario 4 utilizing GDFs from the load test (0.803). It shall be noted that the bridge is load rated based on the current AASHTO MBE [1] and the condition factors for these cases are taken as 1.0.

Table 21. - Summary of Rating Factor Using HL-93 (Bridge #1412-178)

		Inventory	Operating
As-Built (28 tendons)	Flexure	1.96	2.54
	Shear	2.82	3.65
As-Built*(28 tendons)	Flexure	2.03	2.63
	Shear	2.96	3.84
Minimum Design (18 tendons)	Flexure	1.26	1.63
	Shear	1.40	1.81
Maximum Design (36 tendons)	Flexure	2.32	3.01
	Shear	1.20	1.56
Minimum Design (18 tendons)*	Flexure	1.30	1.68
	Shear	1.68	2.19
Minimum Design (18 tendons)**	Flexure	1.58	2.05
	Shear	-	-

*compressive strength from Schmidt Hammer is used

**compressive strength from Schmidt Hammer and GDFs (moment) from test result are used

For proposed method, it can be seen from the Table 21 that:

1. The Minimum Design still has a rating factor greater than 1.0, which meets the NJDOT requirement.

2. The bridge originally designed with twenty-eight (28) tendons has a Minimum Design with Eighteen (18) tendons. The ten (10) more tendons shows the capacity reserve of the structure.
3. The trend of operating level is consistent with that of inventory level.
4. The compressive strength updating will increase the rating factor for both strength and shear capacity, while the increase in shear is greater than that in flexure.
5. Comparing the Minimum Design and the case of Minimum Design with GDFs from testing, an increase of 21.5% in flexure rating factor for inventory level is found.
6. In this case, comparing the shear rating between Minimum Design and Maximum Design, the Maximum Design has a lower rating. It is because that increasing the tendon number does not contribute to the shear resistance. On the opposite, it would decrease the effective shear depth, leading to the decrease in the shear capacity. Also, the effective shear depth will have an effect on the critical section. In this case, the critical section is moving closer to the support, where the shear force is greater. te

4.5. Capacity Comparison in Bridge Inventory

4.5.1. Bridge Inventory and Re-design

The developed load rating procedure is applied on more bridges from the inventory when plans are available. It should be noted that the Schmidt Hammer and diagnostic load test were not performed on these bridges. The results are shown in Figure 41 to Figure 49. The

summary of rating factor, calculated based on scenarios 1) as specified in the inspection report, 2) the bridge is redesigned with minimum requirement of tendons using as-built design load and 3) the bridge is re-designed with maximum requirement of tendons using as-built design load. The results are shown through Table 22 to Table 28.

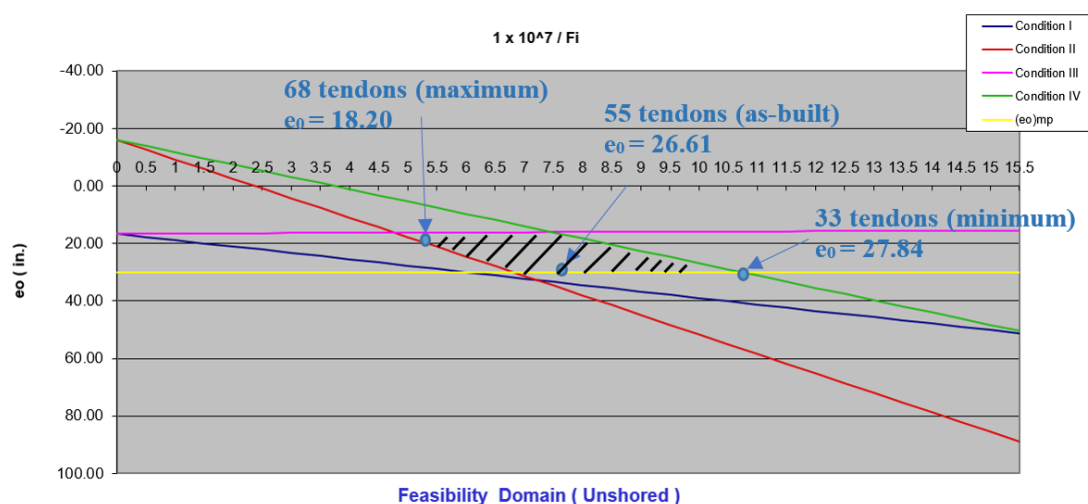


Figure 41. Feasibility Domain for #0235-157

Table 22. Summary of Rating Factor Using HL-93 (Bridge #0235-157)

		Inventory	Operating
As-built plan (55 tendons)	Flexure	2.38	3.09
	Shear	4.28	5.55
Minimum Design (33 tendons)	Flexure	1.10	1.42
	Shear	-	-
Maximum Design (68 tendons)	Flexure	2.59	3.36
	Shear	-	-

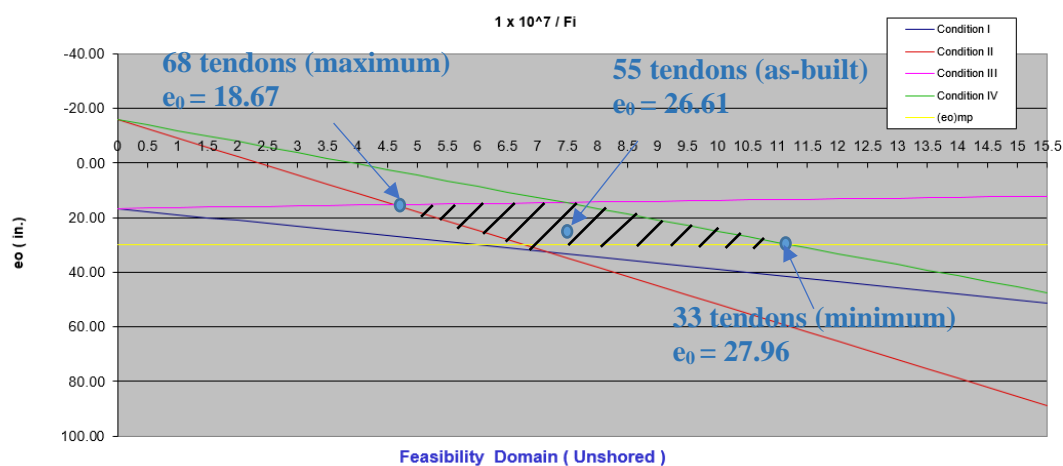


Figure 42. Feasibility Domain for #0235-156

Figure 43. Summary of Rating Factor Using HL-93 (Bridge #0235-156)

		Inventory	Operating
As-built plan (55 tendons)	Flexure	2.26	2.95
	Shear	3.90	5.06
Minimum Design (32 tendons)	Flexure	1.00	1.30
	Shear	-	-
Maximum Design (68 tendons)	Flexure	2.35	3.05
	Shear	-	-

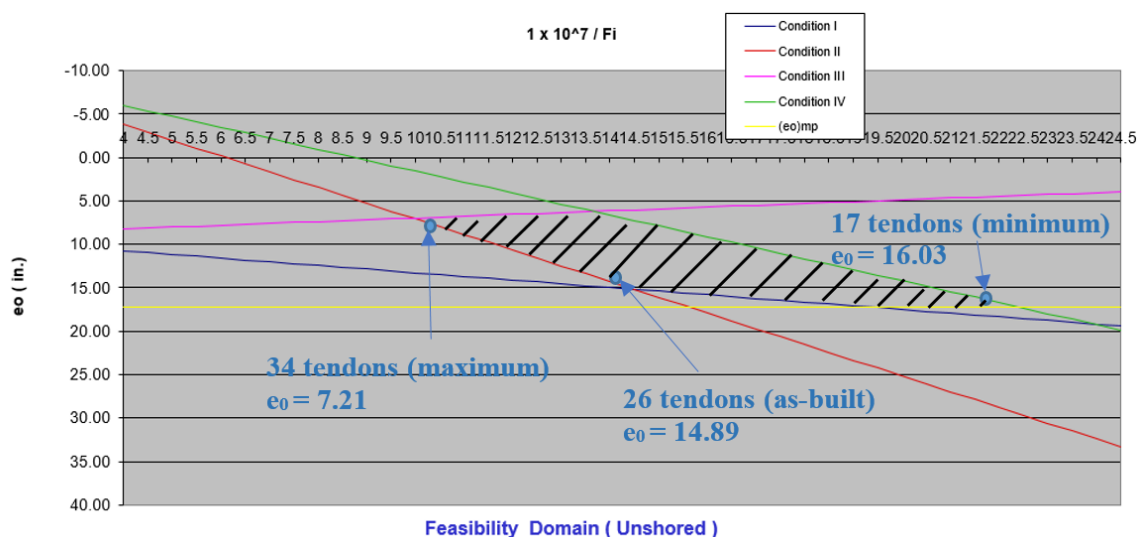


Figure 44. Feasibility Domain for #1420-168 middle span

Table 23. Summary of Rating Factor Using HL-93 (Bridge #1420-168, middle span)

		Inventory	Operating
As-built plan (26 tendons)	Flexure	2.02	2.62
	Shear	3.03	3.93
Minimum Design (17 tendons)	Flexure	1.19	1.55
	Shear	-	-
Maximum Design (34 tendons)	Flexure	2.16	2.85
	Shear	-	-

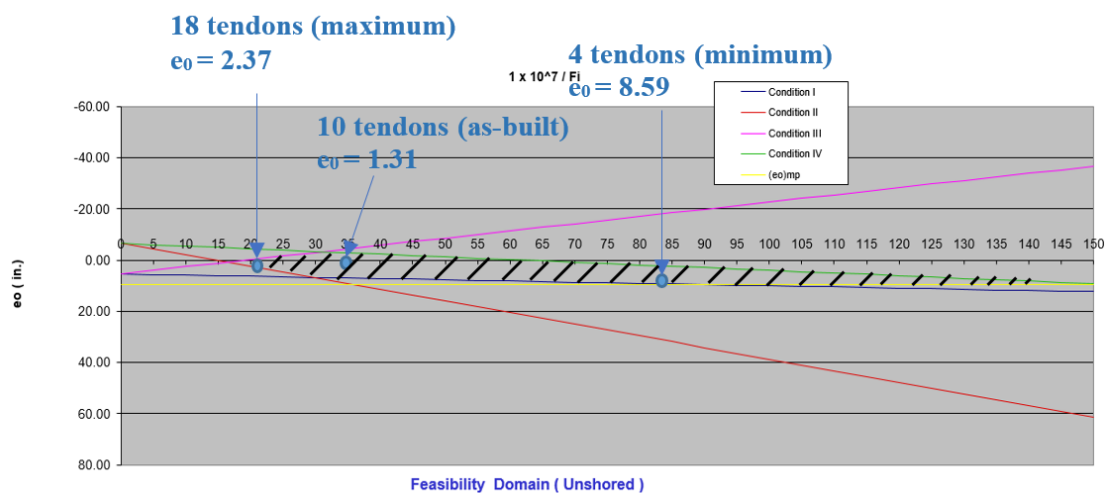


Figure 45. Feasibility Domain for #1420-168 end span

Table 24. Summary of Rating Factor Using HL-93 (Bridge #1420-168, end span)

		Inventory	Operating
As-built plan (10 tendons)	Flexure	2.35	3.05
	Shear	4.37	5.67
Minimum Design (4 tendons)	Flexure	1.13	1.46
	Shear	-	-
Maximum Design (18 tendons)	Flexure	4.48	5.81
	Shear	-	-

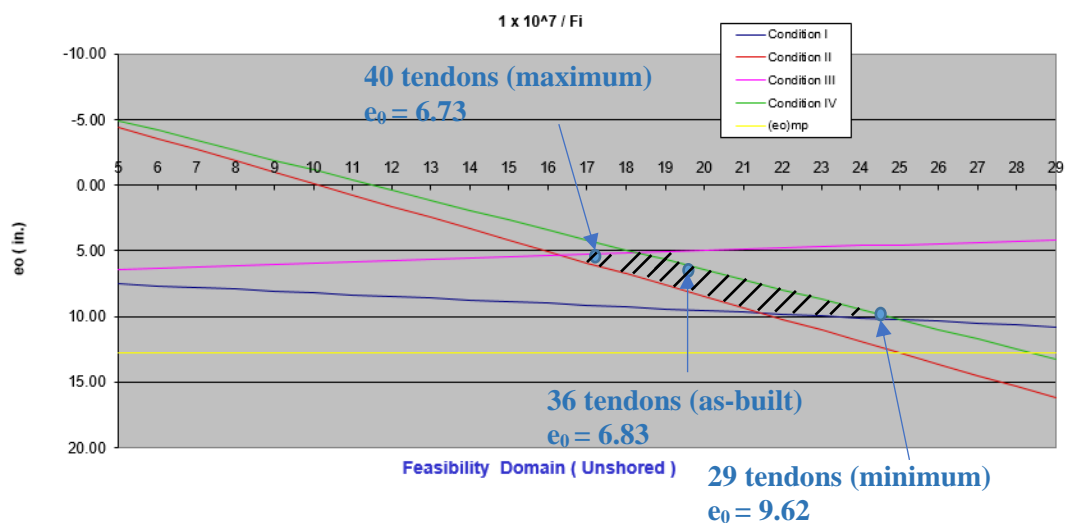


Figure 46. Feasibility Domain for #1413-156

Table 25. Summary of Rating Factor Using HL-93 (Bridge #1413-156)

		Inventory	Operating
As-built plan (36 tendons)	Flexure	1.45	1.89
	Shear	3.46	4.49
Minimum Design (29 tendons)	Flexure	1.23	1.60
	Shear	-	-
Maximum Design (40 tendons)	Flexure	1.64	2.13
	Shear	-	-

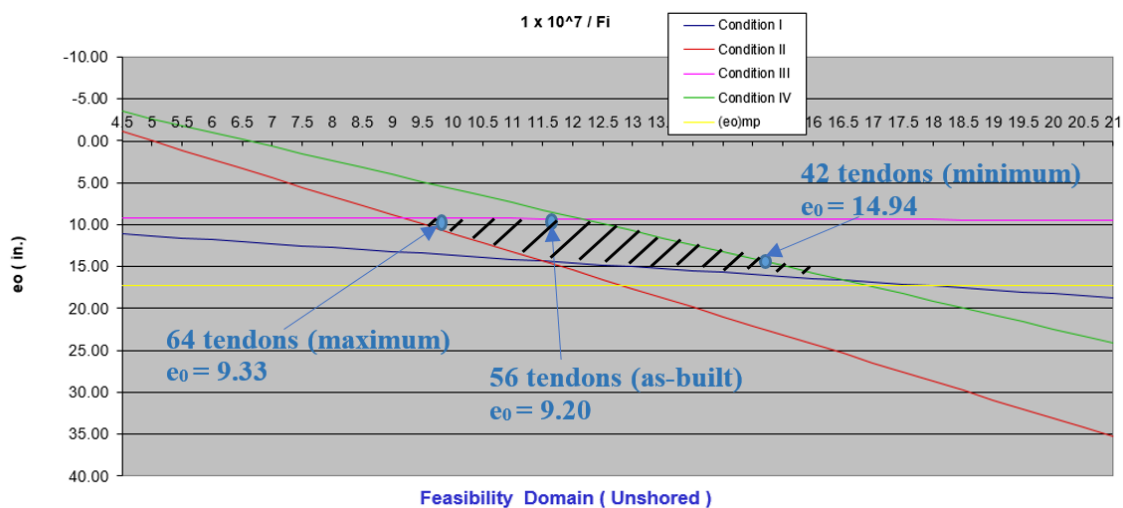


Figure 47. Feasibility Domain for #0327-150

Table 26. Summary of Rating Factor Using HL-93 (Bridge #0327-150)

		Inventory	Operating
Inspection Report (56 tendons)	Flexure	1.68	2.18
	Shear	2.64	3.42
Minimum Design (42 tendons)	Flexure	1.37	1.78
	Shear	-	-
Maximum Design (64 tendons)	Flexure	2.04	2.64
	Shear	-	-

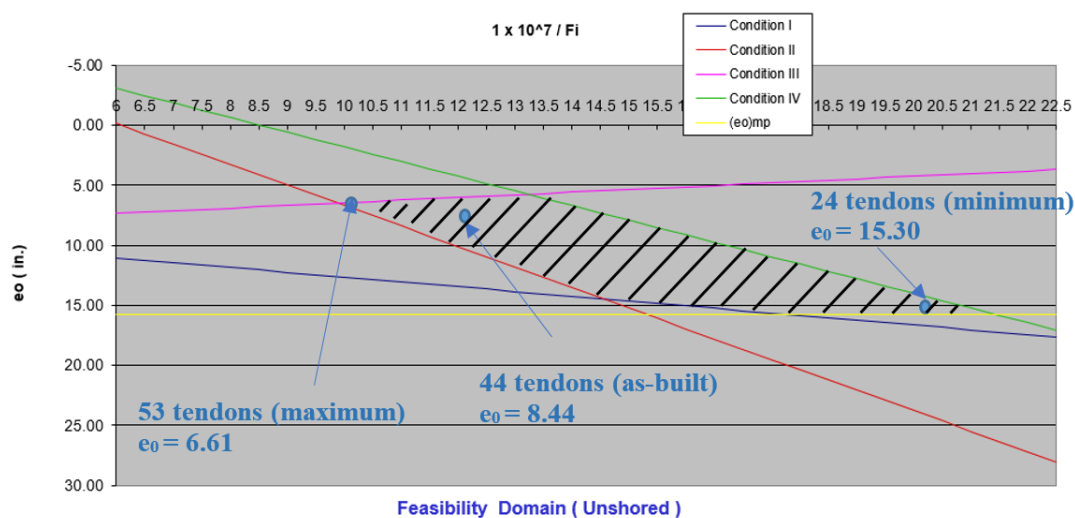


Figure 48. Feasibility Domain for #1016-159

Table 27. Summary of Rating Factor Using HL-93 (Bridge #1016-159)

		Inventory	Operating
As-built plan (44 tendons)	Flexure	1.94	2.52
	Shear	0.53	0.69
Minimum Design (24 tendons)	Flexure	1.09	1.41
	Shear	-	-
Maximum Design (53 tendons)	Flexure	2.27	2.94
	Shear	-	-

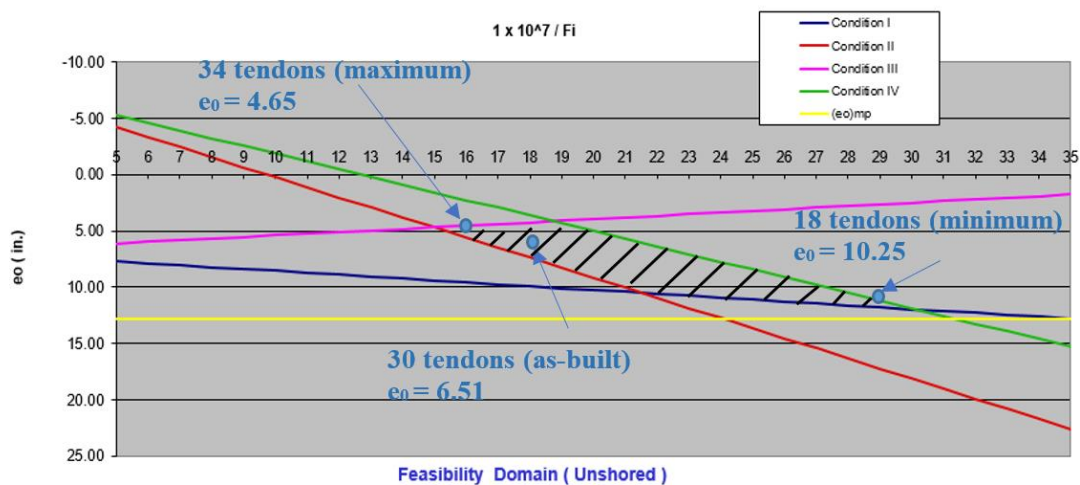


Figure 49. Feasibility Domain for #2113-153

Table 28. Summary of Rating Factor Using HL-93 (Bridge #2113-153)

		Inventory	Operating
As-built plan (30 tendons)	Flexure	1.88	2.44
	Shear	2.00	2.60
Minimum Design (18 tendons)	Flexure	1.15	1.50
	Shear	-	-
Maximum Design (34 tendons)	Flexure	2.01	2.60
	Shear	-	-

4.5.2. Bridge Inventory and Profile

The profile of the redesign and as-built cross-section for bridge inventory are shown through Figure 50 to Figure 58.

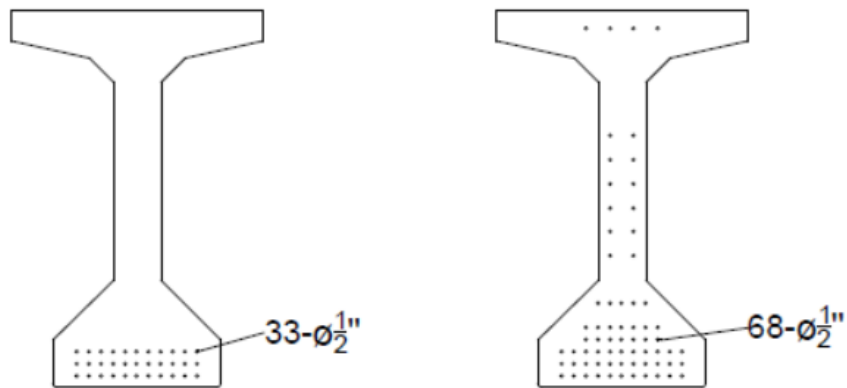


Figure 50. AASHTO Type V # 0235-157

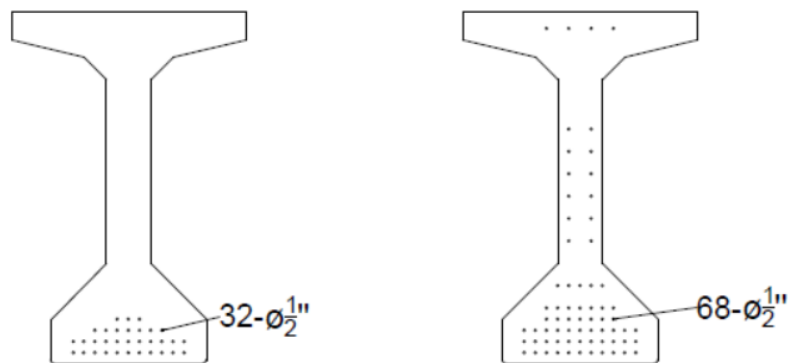


Figure 51. AASHTO Type V # 0325-156



Figure 52 AASHTO Type II # 1412-178

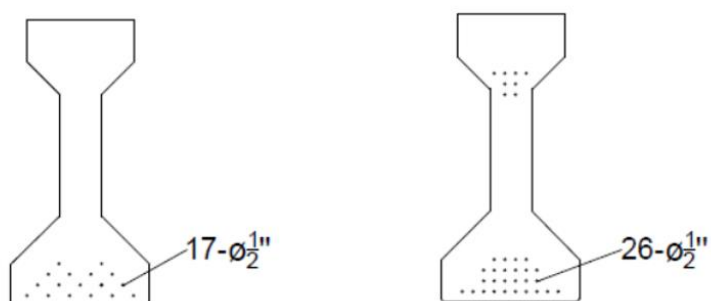


Figure 53. AASHTO Type III # 1420-168 Middle Span



Figure 54. AASHTO Type I # 1420-168 End-Span



Figure 55. AASHTO Type II # 1413-156

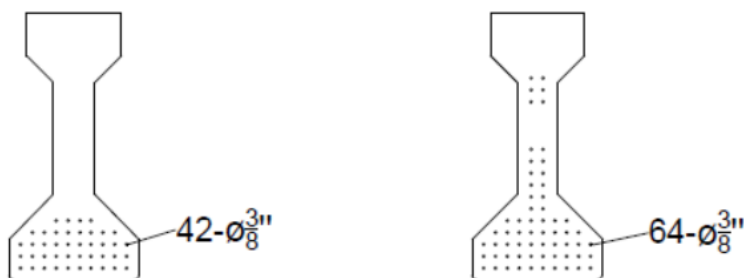


Figure 56. AASHTO Type II # 0327-150

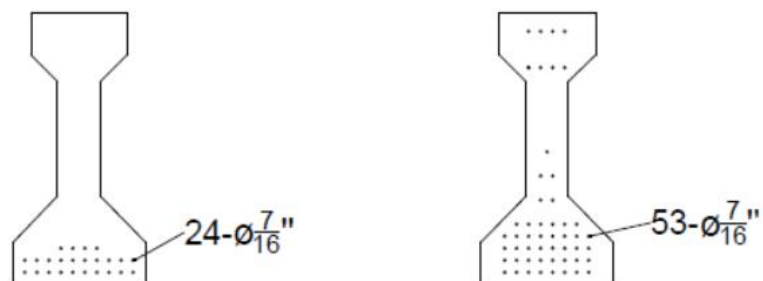


Figure 57. AASHTO Type II # 1016-159



Figure 58. AASHTO Type II # 2113-153

4.5.3. Capacity Comparison

Table 29 summarizes the structure number and the capacity of each bridge. The capacity difference between maximum design and minimum design as well as the difference between as-built design and minimum design are calculated based on the bridge inventory. For the difference between Maximum design and Minimum design, the percentage is calculated using equation (11).

$$\frac{\text{Maximum Capacity} - \text{Minimum Capacity}}{\text{Minimum Capacity}} \quad (11)$$

The difference between As-built design and Minimum design shows the safety range added to the minimum design when the designer designed the bridge. The percentage is calculated using equation (12).

$$\frac{\text{As - built Capacity} - \text{Minimum Capacity}}{\text{Minimum Capacity}} \quad (12)$$

The portion of safety range within the feasibility domain shows the percentage of safety applied to the feasibility domain when the designer designed the bridge. It is calculated using equation (13).

$$\frac{\text{Difference between Minimum and As - built}}{\text{Difference between Minimum and Maximum}} \quad (13)$$

Table 29. Summary of Structure and Capacity

SN.	Minimum Capacity (Kip-ft)	Maximum Capacity (Kip-ft)	Difference between Maximum design and Minimum design	As-Built Capacity (Kip-ft)	Difference between As-Built design and Minimum design	The Portion of Safety Range within the Feasibility Domain
1412-178	1515	2434	60.7%	2121	40.0%	65.9%
0235-157	7427	11714	57.7%	11425	53.8%	93.3%
0235-156	6770	10908	61.1%	10678	57.7%	94.4%
1420-168 Mid Span	2806	4280	52.5%	4062	44.8%	85.2%
1420-168 End Span	456	1538	237.3%	851	86.6%	36.5%
1413-156	1861	2325	24.9%	2117	13.8%	55.2%
0327-150	3776	4895	29.6%	4331	14.7%	49.6%
1016-159	2838	4861	71.3%	4303	51.6%	72.4%
2113-153	1608	2441	52.4%	2317	44.1%	84.1%

4.6. Analysis of Deteriorated Bridges with No Plans

For a bridge with deteriorated section, the method of analyzing the P/C with no plans was used combining with prestressing section loss. The rating factors were calculated based on LRFR and LFR with HL-93 and HS-20 respectively. From field visit and information in cycle report [10], three (3) bridges with exposed prestress strands were selected for calculating the rating factors. According to NJDOT Bridge Element Inspection Manual [6] for bridges with deterioration, through inspection, if tendons are identified exposed in the bridge, and the condition states is poor (Condition State 3), according to element rating, the structure should be considered with section loss. In this proposed method, it is suggested that the corroded or/and exposed tendon should be removed from calculation to be conservative.

For shear resistance at support, the concrete in the web would contribute to the shear capacity. As for concrete deteriorated section, for girders, the area of spalling and cracking should be measured and considered as section loss.

4.6.1. Field Visit of Bridges with Structural Number 1412-178

From field visit, at the support, the concrete section is deteriorated with spalling and exposed tendon shown in Figure 59 and Figure 60. Two (2) tendons are exposed and Identified as poor condition (Condition State 3) from filed visit. The tendons are taken out from the capacity calculation both in the mid-span and at support, with the assumption that the corroded tendon will not contribute to the flexure resistance.



Figure 59. Deterioration at Support



Figure 60. Exposed Tendons in 1412-178

4.6.2. Analysis of Bridges with Deterioration for #1412-178

For comparison, the rating factors were calculated both for minimum design without deterioration and minimum design with deterioration. The results are shown in Table 30 and Table 31 respectively. The minimum design has eighteen (18) tendons in total and with two (2) deteriorated tendons. The rating factors were calculated based on sixteen (16) tendons.

Table 30. RFs of Minimum Design for 1412-178 without Deterioration (18 tendons)

Limit state	HL-93 (LRFR)		HS-20 (LFR)	
	Inventory RF	Operating RF	Inventory RF	Operating RF
Strength I	-	-	-	-
Flexure (at midspan)	1.26	1.63	1.21	2.02
Shear (at critical)	1.40	1.81	1.35	2.26

Table 31. RFs of Minimum Design for 1412-178 with Deterioration (16 tendons)

Limit state	HL-93 (LRFR)		HS-20 (LFR)	
	Inventory RF	Operating RF	Inventory RF	Operating RF
Strength I	-	-	-	-
Flexure (at midspan)	1.04	1.36	1.01	1.68
Shear (at critical)	1.36	1.81	1.32	2.20

4.6.3. Information in Cycle Report of #1420-168 (End-Span)

From the recent cycle report, the inspection team identified exposed and rusted strands at the support, shown in Figure 61. This information can be used for estimating the strand pattern for minimum design. Since the span length of this bridge is 20.5 ft, the calculated minimum tendon number is only four (4). From exposed tendons, it will give engineer an idea of how tendons distributed in concrete if no plans are available.



Photo No: 19-08

Location:	East fascia beams (Center and North Spans) over North pier, looking Northwest.
Description:	Large spalls (3 SF x 2" deep at each location with exposed and rusted strands on bottom flange and web of the East fascia beams. (Typical at beams B5 and B6 at north pier).

Figure 61. Exposed Tendons in 1420-168 (End-Span)

4.6.4. Analysis of the Bridge with Deterioration for #1420-168 (End-Span)

In this case, no picture directly identified the exposed tendons, thus, the assumption of one tendon is exposed with a condition state of three (3) is made to calculate the rating factors. Results are shown in Table 32 and Table 33. From the results, it shows that the rating factors are below one (1.0). However, based on engineering judgment it is unlikely only

four tendons are used. In the report, both corroded tendons are found in the web and bottom, in this case, clearer pictures are needed to make decisions. Only one (1) tendon were taken out for calculation from bottom. The exposed tendon can give an idea to engineer of the tendon profile.

Table 32. RFs of Minimum Design for 1412-178 without Deterioration (4 tendons)

Limit state	HL-93 (LRFR)		HS-20 (LFR)	
	Inventory RF	Operating RF	Inventory RF	Operating RF
Strength I	-	-	-	-
Flexure (at midspan)	1.13	1.46	1.31	2.18

Table 33. RFs of Minimum Design for 1412-178 with Deterioration (3 tendons)

Limit state	HL-93 (LRFR)		HS-20 (LFR)	
	Inventory RF	Operating RF	Inventory RF	Operating RF
Strength I	-	-	-	-
Flexure (at midspan)	0.77	1.00	0.90	1.50

4.6.5. Analysis of Bridges with Deterioration for #1413-156

From inspection report, one (1) prestressing strand was identified shown in Figure 62. The calculated results are shown in Table 34 and Table 35. From the results, the rating factors are greater than 1.0.


Description:		Wide longitudinal crack with an incipient spall at the east end due to underlying corroded pre-tension strands. Refer to Priority Repair Letter 1413156_20150702cy19_PR01_01 .
		Photo No: P2
Location:		Pre-stressed I-beam, south fascia beam over west abutment.
Description:		Spall at the west end with a corroded pre-tension strand. Refer to Priority Repair Letter 1413156_201500702cy19_PR01_01 .

Figure 62. Exposed Tendons in 1413-156

Table 34. RFs of Minimum Design for 1413-156 without Deterioration (29 tendons)

Limit state	HL-93 (LRFR)		HS-20 (LFR)	
	Inventory RF	Operating RF	Inventory RF	Operating RF
Strength I	-	-	-	-
Flexure (at midspan)	1.23	1.60	1.17	1.95

Table 35. RFs of Minimum Design for 1413-156 with Deterioration (28 tendons)

Limit state	HL-93 (LRFR)		HS-20 (LFR)	
	Inventory RF	Operating RF	Inventory RF	Operating RF
Strength I	-	-	-	-
Flexure (at midspan)	1.172	1.52	1.12	1.86

Chapter IV

5. Conclusions and Summary

5.1. Conclusion

To load rate prestressed concrete bridges without plans, an estimation for load-carrying capacity based on the geometries is needed. The dimensions can be measured easily on site. However, the reinforcement and prestressed tendons are embedded in the concrete, and they contribute a large part to the shear and flexure resistance, respectively. Therefore the capacity is difficult to be determined without those information. In this study, NDT/Es and feasibility domain are used to estimate the information of concrete strength, reinforcement details, and prestressing tendon profiles. This study conservatively calculated the rating factors for nine cases. Based on experimental results, the conclusions are drawn here:

Estimating the strand pattern

- In this study, a sensitivity analysis was performed to calculate the neutral axis. Theoretically, the neutral axis changes correspondingly to the strand pattern. However, the results showed that within the linear elastic range, the neutral axis was not sensitive to the strand numbers. Also, when compared the elastic results from calculation to the actual test results, there was a difference of 4.47 inches (girder G5 path 1). Because of the material uncertainty, it is found that the neutral axis was not sensible for estimating strand pattern.

- Proceq Profoscope+ (rebar locator) was performed on site to scan and estimate the prestressing strand profile and size. By comparing the results to the drawing, the rebar locator gave a significantly larger tendons size than what was specified in the drawing in a congested area. This showed that the Proceq Profoscope could not be used in the field for measurement.
- Re-design the prestress concrete cross-section using the live load according to the time when the bridge was built. Using feasibility domain, and apply the minimum and maximum design for calculating the flexure capacity. A rating factor number can be selected within the range. And to be conservative, the minimum rating factor can be used. Furthermore, a certain safety range could be selected from bridge inventory to apply on the rating factors based on the importance of the bridge and route.

Estimating the shear stirrup

- In this study, GPR (ground penetrating radar) was used to investigate the distribution of stirrups inside the P/C girder. By comparing the results to the drawing plans, it was found that the GPR provided a reasonable estimation of stirrups spacing. However, the size of the stirrup was not provided. For this study, a conservative assumption was made with the size of stirrups being #4 bar. Engineering judgment is needed to determine the size of stirrups due to lack of information from GPR. Based on the year built, the common practical size of stirrup

can be determined. This piece of information is essential for estimating the shear capacity of a structure.

Estimating the concrete compressive strength

- The experiments were conducted inside and outside RIME laboratory to validate the reliability and accuracy of Schmidt Hammer. Based on the experimental results, Schmidt Hammer provided a less conservative compressive strength than what it was specified in the inspection report. The estimated concrete strength from Schmidt Hammer was still lower than the actual strength from compression machine. With the use of Schmidt Hammer, a less conservative, but more realistic, concrete strength can be estimated. With this piece of information, the overall capacity of the structure can be increased.

Diagnostic load test

- The diagnostic load test can be used to safely evaluate the actual responses of the structure. GDF values from the load test were used to validate the GDFs' equations in AASHTO.
- Static load test was preferred for calculating GDF to eliminate the influences caused by impact from other cars. In this study, the dynamic load test was performed to avoid affecting the traffic on the bridge.
- GDF of one-lane loaded was calculated using the strains caused by the truck. Superposition method was used to calculate GDF for two or more lanes loaded. It was found that that GDF's from AASHTO were already conservative.

- Diagnostic load test would be needed when the rating factors calculated by using NDT/Es and the re-design are still not satisfied with the criteria.
- The calibration truck is successfully posted for SN 1412-178.

5.2. Future Work

- The team will apply the proposed methodology using additional bridges with no plans. Those bridges will be selected by NJDOT as a follow-up study.
- The team will apply the proposed methodology to the bridge inventory that has the plans available and clustering the bridges into category. This can identify the capacity reserve for the bridges that have already been built. The values can be used to estimate for a bridge has no plans.
- Similar diagnostic tests would be applied to the bridges with no plans selected by NJDOT. GPR is recommended to be used on more P/C bridges to see the reliability of the test.
- A Finite Element Model can be used calibrated by the field test for updating the shear girder distribution and further analysis.

References

1. American Association of State Highway and Transportation Officials (2011). *Manual for Bridge Evaluation*, 2nd ed. AASHTO, Washington, D.C.
2. Carlos V. Aguilar, David V. Jáuregui, Craig M. Newton, Brad D. Weldon, and Tamara M. Cortez (2015). *Load Rating a Prestressed Concrete Double T-Beam Bridge without Plans by Field Testing*. Transportation Research Board, Washington, D.C.
3. Rafal Anay; Tamara M. Cortez; David V. Jáuregui, M.ASCE; Mohamed K. ElBatanouny; and Paul Ziehl (2015). *On-Site Acoustic-Emission Monitoring for Assessment of a Prestressed Concrete Double-Tee-Beam Bridge without Plans*. Journal of Performance of Constructed Facilities, American Society of Civil Engineers.
4. Carlos V. Aguilar, David V. Jáuregui, Craig M. Newton, and Brad D. Weldon (2015). *Implementation Plan for Load Rating Prestressed Concrete Bridges without Plans*. Maintenance, Monitoring, Safety, Risk and Resilience of Bridges and Bridge Networks.
5. Joan R. Casas, Piotr Olaszek, Aljoša Šajna, Aleš Žnidarič, Igor Lavrič (2009). *Recommendations on the use of soft, diagnostic and proof load testing* Sustainable Development, Global Change and Ecosystems Sustainable Surface Transport
6. New Jersey Department of Transportation (2014). *Bridge Element Inspection Manual* Structural Evaluation & Bridge Management, Trenton, NJ.
7. Wisconsin Department of Transportation (WisDOT). (2017). *WisDot Bridge Manual Chapter 45*. Madison, WI.
8. The PCI Bridge Design Manual Steering Committee, part of the Transportation Activities Council. *Bridge Design Manual Precast Prestressed Concrete 3rd edition* Precast/Prestressed Concrete Institute.
9. Wassef, W., Smith, C., Clancy, C., & Smith, M. (2003). *Comprehensive Design Example for Prestressed Concrete (PSC) Girder Superstructure Bridge with Commentary*. Federal Highway Administration report no. FHWA NHI-04-043, grant no. DTFH61-02-D-63006. Washington, DC: US Government Printing Office.
10. New Jersey Department OF Transportation (NJDOT). (2012). *Bridge Re-Evaluation Survey Report Structure No. 1412-178 17th cycle*. Trenton, NJ.

11. American Association of State Highway and Transportation Officials (2012). *LRFD Bridge Design Specifications*. Washington, D.C.
12. Hag-Elsafi, Osman, and Jonathan Kunin. (2006). *Load Testing for Bridge Rating: Dean's Mill Over Hannacrois Creek*. No. FHWA/NY/SR-06/147. Report FHWA/NY/SR-06/147. Transportation Research and Development Bureau, New York State Department of Transportation, Albany.
13. Naaman, A. E. (1982). *Prestressed concrete analysis and design: fundamentals*. New York, McGraw-Hill.